complexities

MDPI

Article

Thermodynamic Description of Wealth Inequality in the World

Klaus M. Frahm [1], Leonardo Ermann [2] and Dima L. Shepelyansky [1,*]

[1] Laboratoire de Physique Théorique, Université de Toulouse, CNRS, 31062 Toulouse, France
[2] Departamento de Física Teórica, GIyA, Comisión Nacional de Energía Atómica, Av. del Libertador 8250, Buenos Aires 1429, Argentina
* Correspondence: dima@irsamc.ups-tlse.fr; Tel.: +33-56155-60-68

Abstract

According to the recent Wealth Thermalization Hypothesis (WTH), the wealth inequality in the world is described by the Rayleigh–Jeans (RJ) thermal distribution of interacting agents in a society with social stratification. In this concept, the wealth layers of society are associated with energy levels from a nonlinear dynamical system conserving two integrals of motion—namely, total energy and the probability norm. This leads to RJ condensation and the formation of a huge poverty phase of low wealth and a tiny oligarchic phase that captures a main part of total society wealth. This RJ phenomenon has similarities with self-cleaning in multimode optical fibers and constraint-driven condensation in various physical systems. We analyze real Lorenz and Pareto curves for wealth of households in countries and the world; gross domestic product of countries; market capitalization of companies on the stock exchanges of Hong Kong, Shanghai, and London; bitcoin transactions; and world trade between countries and show that the WTH theory gives a good description of these curves. On the basis of this comparison, we argue that the RJ thermal distribution provides a universal description of wealth inequality in the world.

Keywords: Rayleigh–Jeans thermalization; wealth inequality; Lorenz and Pareto curves; GDP; stock exchange markets; bitcoins

1. Introduction

Statistical mechanics finds enormously broad applications in various fields of science (see, e.g., [1]). Thermodynamic probability distributions for many degrees of freedom describe numerous physical systems including the black-body cosmic microwave background in the Universe, where the Bose–Einstein distribution is amazingly accurate, with deviations of less than 10^{-3} in relative units (see, e.g., [2,3]). The application of ideas and methods of statistical mechanics to economy and finance became known as econophysics [4]. In this context, arguments for the Boltzmann–Gibbs distribution of money, wealth and income in human society, also based on real data, have been presented in stimulating reviews on applications of statistical mechanics in economy [5,6].

The striking feature of the wealth distribution of world countries is the strong inequality of wealth of households, as reviewed, e.g., in [7–9]. Indeed, according to [8], for the whole world, 50% of the population owns only 2% of total wealth, while 10% of the population owns 75% of total wealth and 1% of the population owns 38% of total wealth.

Various approaches based on statistical mechanics and physical kinetics [1,10] have been used by different research groups [5,6,11–16] to explain the phenomenon of wealth inequality. Diverse models of interacting agents have been investigated, including Random asset exchange models. In certain of these models, there is the appearance of some kind

Check for updates

Academic Editors: Lock Yue Chew, François Gay-Balmaz and José F. F. Mendes

Received: 16 June 2026
Revised: 24 August 2026
Accepted: 4 September 2026
Published: 8 September 2026

Copyright: © 2026 by the authors. Licensee MDPI, Basel, Switzerland. This article is an open access article distributed under the terms and conditions of the Creative Commons Attribution (CC BY) license.

of oligarchic phase with a significant wealth accumulation by a group of agents [13,15,16]. Different arguments have been presented in favor of the Boltzmann–Gibbs-type description of the distribution of money, wealth and income in [5,6]. A nonlinear Fokker–Planck description of asset exchange is pushed forward in [15,16], with the emergence of an oligarchic phase. The importance of two conserved integrals of system evolution is stressed in [15,16]. These integrals are the total wealth and total probability norm (or number of agents). Furthermore, it was argued that in the small-transaction approximation, it is important to consider wealth instead of money or income.

An efficient description of wealth distribution is known as the Lorenz curve [9,17] which represents the dependence of cumulated normalized wealth ($0 \leq w \leq 1$) on the cumulated normalized fraction of population or households ($0 \leq h \leq 1$). The case of perfect equipartition of wealth corresponds to the diagonal ($w = h$), and the doubled area between the diagonal and the Lorenz curve ($w(h)$) gives the Gini coefficient ($0 \leq G \leq 1$) [9,18]. Typical values of the Gini coefficient (G) are presented in the range of $0.59 < G < 0.90$ in [19] for world countries in 2021; for the whole world, $G = 0.889$ (these data come from the Global Wealth Databook by Credit Suisse). High values of the Gini coefficient close to unity correspond to high inequality in a country with a large fraction of poor population and a tiny oligarchic population fraction that owns a huge fraction of total wealth [7,8].

Recently, the Wealth Thermalization Hypothesis (WTH) was proposed in [20], with the aim of explaining the origins of such universal wealth inequality existing in countries and the whole world. The WTH argues that various types of links and nonlinear interactions between society members (agents) in a given country lead to dynamical thermalization over layers of Social Stratification in a Society (SSS). This SSS is characterized by wealth values (w_m) of corresponding layer states with approximately constant density of states ($\nu = dm/dw_m = const$). The appearance of SSS is broadly discussed in social science starting from the Marxist theory of classes (see, e.g., [21–25]). Using a mathematical SSS model, it was shown in [26] that links between agents (m) and their nonlinear interactions lead to dynamical chaos and Rayleigh–Jeans (RJ) thermalization. In fact, the wealth values (w_m) can be considered as energies (E_m) of states (m) (or related frequencies). As argued in [15,16], the thermalization process has two conserved quantities—total system energy ($E = \sum_m E_m \rho_m$) and the probability norm ($\eta = \sum_m \rho_m$), i.e., the number of agents, where ρ_m is the time-averaged squared amplitude and occupation probability of each oscillator mode (m) considered in [26]. According to the well known results of thermodynamics of classical fields [1,27] the steady-state distribution of probabilities (or fractions) for the RJ thermalization has the following form:

$$\rho_m = \frac{T}{E_m - \mu} \text{ (RJ)}. \tag{1}$$

Here, ρ_m represents averaged stationary probabilities at certain wealth states ($0 \leq m < N$) with wealth/energies ($w_m = E_m$). The two parameters correspond to the system temperature (T) and the chemical potential ($\mu(T)$), which are determined by the values of total energy (E) and norm $\eta = 1$ via both equations given above. (See, e.g., Refs. [20,26,28] and below for more details.)

The RJ distribution also follows from the Bose–Einstein thermal distribution of quantum bosonic fields at high temperatures ($T \gg E_m - \mu$) [1]:

$$\rho_m = \frac{1}{\exp[(E_m - \mu)/T] - 1} \text{ (BE)}. \tag{2}$$

It has been shown that the dynamical RJ thermalization appears in systems such as SSS models [26], nonlinear perturbation of Random Matrix Theory (RMT) [28], social

networks [20], and light propagation in multimode optical fibers [29]. This thermalization results from chaotic dynamics emerging when a nonlinearity parameter exceeds a certain chaos border [30,31]. Below the chaos border, the dynamics are integrable in the main part of the phase space, in agreement with the Kolmogorov–Arnold–Moser (KAM) theorem [32,33].

In fact, RJ thermalization has been studied experimentally and numerically for light propagation in nonlinear media of multimode optical fibers [34–40]. However, the origins of RJ thermalization were never clarified, and it is absent at weak nonlinearity below the chaos border when the dynamics become integrable, as stated by the KAM theorem. At the same time, analytical studies and numerical simulations of the Nonlinear Schödinger Equation (NSE) for light propagation [35] showed that at moderate nonlinearities and low energy injected in the system, the RJ thermal distribution (1) leads to an enormous condensation of total probability at the fiber ground state, with about 80–90% of probability in this state. This phenomenon, called self-cleaning, was experimentally demonstrated for fibers in [34,37]. RJ condensation was also found in the NSE numerical modeling of light propagation in D-shaped quantum chaos fibers [29].

Actually, the RJ condensation follows directly from the RJ thermal distribution (1) and two integrals of motion—energy (E) and norm (η)—that can be considered two constraints. Then, it is easy to show that at a low temperature ($T \sim E_g$), a huge macroscopic probability ($\rho_g \to 1$) is condensed at the ground state ($m = 0$) with energy of $E_g = E_0$. Examples of such condensation in the RJ standard (RJS) model with equidistant energy states ($E_m = \nu m$) ($0 \leq m \leq N-1$)) and constant density of states ($\nu = dm/dE_m = const$) are given in [20,29]. According to the WTH, the wealth inequality of households in countries results from this RJ thermal condensation when the total wealth (energy) of a country is small compared to the wealth dispersion (B) in the society, where $B = E_{max} \approx N/\nu$ is determined by the maximal wealth of households in a country.

We note that the first results for RJ condensation at low energy modes were obtained by H. Fröhlich in 1968 from (1) for electric modes in biocells [41,42]. However, his analysis contained a logical gap, since it was motivated by the quantum BE distribution (2), making a transition to the RJ case (1) assuming a high-temperature regime with $T \gg E_0, E_1$, yielding RJ condensation in (1), which exists only at $T \sim E_0, E_1$. Also in [41,42], it is assumed that in the system, there are external energy pumping and absorption so that the relation to the case of the conservative RJ thermalization is not so direct (see discussion in [29]). More recently, the emergence of RJ condensation from (1) was established in 2005 for nonlinear waves in NSE [35]. In these works (see e.g., [35,36]), the origins of RJ thermal distribution were attributed to Kolmogorov–Zakharov (KZ) turbulence [27,43].

RJ condensation was experimentally observed in multimode optical fibers in [34,37]. For the NSE in a quantum chaos fiber, it was shown [29] that RJ condensation takes place in a pure Hamiltonian dynamical system due to dynamical chaos above the chaos border, while below this border, there is no thermalization and dynamics are integrable, in agreement with the KAM theorem. Thus, energy pumping and absorption, which are essential for KZ turbulence, are now required, and RJ condensation appears in a purely Hamiltonian system.

De facto, RJ condensation is a specific case of a more generic phenomenon known in statistical mechanics as constraint-driven condensation [44–46]. This condensation is universal and exists for continuous systems such as coalescence in granular media, jamming in traffic, gelation in networks [45] and financial data analysis [46]. Due to this universality, we argue that RJ condensation is at the origin of wealth inequality in countries, the whole world and other society organizations. We illustrate this universality, showing that RJ thermalization and condensation give a good description of real Lorenz curves not only for wealth of households in countries but also for the Gross Domestic Product

(GDP) of countries; market capitalization of companies on the stock exchanges of Hong Kong, London, New York, and Shanghai; bitcoin distribution between wallets (users); and world trade between countries. The appearance of dynamical RJ thermalization due to linear links and nonlinear interactions between agents has been demonstrated for the SSS models [26], nonlinear perturbation of RMT [28], social networks [20] and NSE evolution in quantum chaos fibers [29]. Therefore, we use the RJ expression (1) as given and compare the Lorenz curves from this thermal distribution with the real Lorenz curves for the wealth inequality in the world. We also discuss the properties of the Pareto distribution at very high wealth values.

In this work, we discuss the proposed WTH approach. We do not claim to prove the WTH, but we present a great variety of different systems (wealth in countries, GDP of countries, market capitalization of stock exchanges, bitcoin transactions, and world trade) that are in agreement with the WTH on a time scale of half a century. The various thermodynamic properties and foundations of RJ thermalization, including properties of entropy, are discussed in books of statistical physics (see Refs. [1,27] and published Refs. [20,26,28,29]), and we do not repeat them here.

The article is composed as follows: Section 2 recalls the properties of the RJ thermal distribution and the construction of associated Lorenz and Pareto curves, the WTH description of Lorenz curves of households of countries and the world is given in Section 3, the GDP Lorenz curves are analyzed in Section 4, the WTH description of data of stock exchange markets is presented in Section 5, bitcoin transactions are studied in Section 6, analysis of the world trade data from UN COMTRADE is presented in Section 7, the universality of the thermodynamic description is highlighted in Section 8 and the conclusion is given in Section 9. Additional data and detailed analytical results for two specific RJ models in the continuous limit ($N \to \infty$) are given in the Appendices A–C.

2. Properties of RJ Thermal Distribution and Condensation—Implications for Lorenz and Pareto Curves

2.1. Features of RJ Distribution

In this work, we consider two specific model spectra for the linear oscillator modes (E_m). The first one is the RJS model with equidistant modes ($E_m = m/N$, $m = 0, 1, \ldots, N-1$) with constant density of states ($\nu_{\rm RJS} = dm/dE_m = N$), and the second one is called the RJ Extended (RJE) model with a parameter (a) and $E_m = (e^{am/N} - 1)/(e^a - 1)$. Both have a bandwidth of $B = E_{N-1} - E_0 \approx 1$ (note that in previous work [20,26], we used the RJE model with a different bandwidth of $B > 1$, which does not affect the construction of Lorenz curves; see below for details). The RJE model appears rather natural, since its density of states decreases (for $a > 0$) at high energies (wealth) values (E_m) according to the following:

$$\nu_{\rm RJE}(E_m) = \frac{dm}{dE_m} = \frac{N(e^a - 1)}{a(1 + (e^a - 1)E_m)}, \tag{3}$$

which we consider more realistic when we want to describe real datasets.

In the limit expressed as $a \to 0$, we recover the RJS model, while with increasing a, the exponential growth of E_m becomes more dominant. We will see that the RJE model gives typically a better description of real Lorenz and Pareto curves.

First, we recall the basic RJ thermalization properties for generic spectra with a few figures for the RJS model as an illustration. Let us assume that we have N linear classical oscillators with individual energies of E_m, $m = 0, \ldots, N-1$ (e.g., a spectrum according to the RJS or RJE model), which are coupled by some small, non-linear perturbation (see

Refs. [20,26,28,29] for examples) such that there are two conserved quantities, i.e., the global (squared) amplitude and total energy:

$$\eta = \sum_{m=0}^{N-1} \rho_m = 1 \quad , \quad E = \sum_{m=0}^{N-1} E_m \rho_m \tag{4}$$

where ρ_m is the time-averaged squared amplitude and occupation probability of each oscillator. If the nonlinear terms are weak or moderate (but above a certain chaos border) or if there is some weak coupling to an external system (which respects both constraints (4)), one can assume that the system is thermalized. Applying the framework of the grand canonical ensemble, one introduces two parameters—temperature (T) and chemical potential (μ)—to satisfy both constraints (4) on average, and it can be shown (see, e.g., Ref. [28]) that

$$\rho_m = \frac{T}{E_m - \mu} \quad , \quad T = \frac{E - \mu}{N}, \tag{5}$$

where the expression for the temperature (T) is obtained from $\sum_m (E_m - \mu)\rho_m = (E - \mu)$, which follows directly from (4). The chemical potential is determined (using standard numerical techniques) by solving the implicit equation:

$$1 = \frac{E - \mu}{N} \sum_{m=0}^{N-1} \frac{1}{E_m - \mu} \tag{6}$$

which allows for one physical solution of μ outside the energy interval of $[E_{\min}, E_{\max}]$ with either $\mu < E_{\min}$ ($T > 0$) or $\mu > E_{\max}$ ($T < 0$) (depending on the value of E, we have either $T < 0$ or $T > 0$) such that $\rho_m > 0$. Without going into the details, we mention that for the limiting case of $|\mu| \to \infty$, corresponding to $|T| \to \infty$, one can work out a simplified explicit approximate expression of μ (as a function of E and E_m), showing that the transition from $T > 0$ ($\mu < E_{\min}$) to $T < 0$ ($\mu > E_{\max}$) appears exactly at the critical energy of $E = E_C = (\sum_m E_m)/N$ ("center of mass" of the spectrum (E_m)). In this work, we will only focus on the case of $T > 0$ with $E < E_c$, which is the most important case to fit the real data (e.g., of the World Lorenz curve).

The data from the RJ distribution (1) presented in this work were obtained by this procedure for two different model spectra and certain values of $N = 10{,}000$. Concerning the RJS model, we also considered the cases of $N = 100$ and $N = 1000$ and verified that the obtained Lorenz curves are very close (in graphical precision). In Appendix A Equation (A2), we also present an analytic theory of the RJS (RJE) model in the continuous limit of $N \to \infty$ with explicit formulas for key quantities (e.g., Lorenz curves, Gini coefficient, etc.; see below for details) in terms of the chemical potential, which is determined by a specific implicit equation. The results for $N \to \infty$ are very close to the case of finite $N = 10^4$.

Figure 1 shows, for the RJS model, the dependence of T and μ on $\varepsilon = E/B \approx E$. Note that the left panel shows the rescaled temperature (NT), since typical numerical values of T are $\sim 1/N$ due to the finite value of B in our particular model. The figure illustrates that $-\mu \to 0$ ($\mu \to -\infty$) for $\varepsilon \to 0$ ($\varepsilon \to \varepsilon_C = 1/2$).

Using (6), one can show (for a finite N) that $-\mu \approx E/(N-1) \ll E$ for very small energies ($0 < E \ll 1/N$), and in this particular case, we have $\rho_0 \approx 1$ (strong condensation) and other $\rho_m \sim E/(NE_m) \ll 1/N$ (for $m > 0$). With increasing values of E (or ε), the values of "$-\mu$" increase, and more probability is shifted to the other ρ_m values for $m > 0$. At $\varepsilon \approx 1/2$, we have very large values of "$-\mu$" (and of T) such that all $\rho_m \approx 1/N$ are uniformly constant. A further increase in ε enters the regime of negative temperatures (with $\mu > E_{\max}$) , with possible condensation at the last oscillator with $\rho_{N-1} \gg 1/N$ (in this work, we do not consider the regime of $T < 0$). These features are visible in both

Figures 2 and 3, showing ρ_m versus E_m/B for different values of ε (as a color plot or curves on a logarithmic scale). The effect of condensation for small ε values with a finite macroscopic probability ($\rho_0 \gg 1/N$) is clearly visible in both figures, and qualitatively, one could even say that it extends even up to $\varepsilon = 0.2$ with $\rho_0 = 0.002495$, which is still larger than $1/N$. However, there are also some other values of ρ_m with small m values that are significantly larger than $1/N$ (as can be seen in Figure 3 for the first 5% of modes with $\rho_m \geq 3/N$). The coarse-grained average value at the first 5% of modes at $\varepsilon = 0.2$ is roughly 0.35 times the maximal coarse-grained value at $\varepsilon \approx 0$ (according to Figure 2). This effect corresponds to (modest) condensation on several modes or on a given small mode interval.

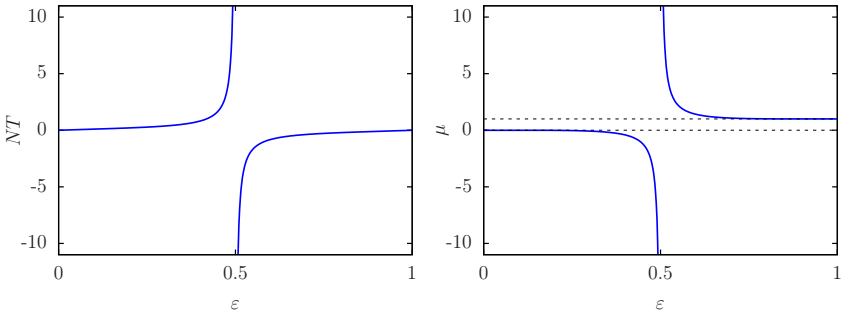


Figure 1. The (**left**,**right**) panel shows the (rescaled or normalized) temperature NT (the chemical potential (μ)) versus the rescaled energy ($\varepsilon = E/B$) for the RJS model ($E_m = m/N$, $N = 10{,}000$). The dashed black lines in the **right panel** correspond to the values of $E_0 = 0$ and $B \approx 1$, showing that either $\mu < E_0$ (for $T > 0$) or $\mu > B$ (for $T < 0$).

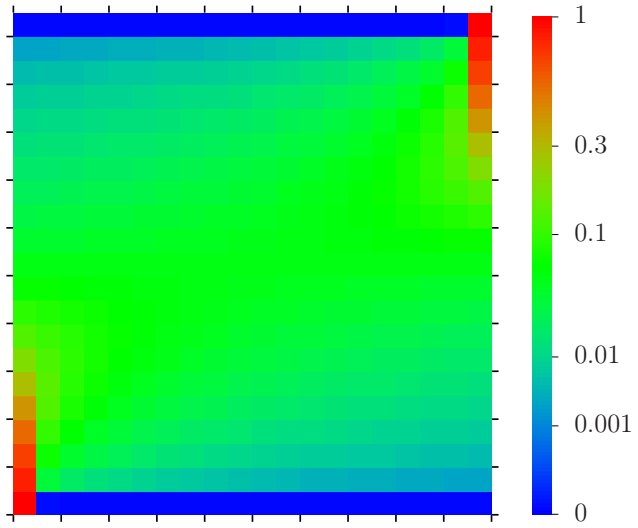


Figure 2. Color plot of the coarse-grained thermalized occupation probabilities ($\rho_m = T/(E_m - \mu) = (E - \mu)/[N(E_m - \mu)]$) for the RJS model. The x-axis corresponds to the fraction expressed as $E_m/B \in [0, 1]$ (left to right), and the y-axis corresponds to the rescaled energy (ε, top to bottom for increasing values). The ticks indicate integer multiples of 0.1 for both quantities. The color values shown in the color bar correspond to the value of ρ_m averaged over intervals of size $1/20$. To increase the visibility of small values, a non-linear color-bar scale is used (e.g., green color corresponds to $1/16$).

2.2. Construction of the Lorenz Curve for RJ Models

To construct the Lorenz curve for a generic RJ model such as the RJS or RJE model, we need to define the cumulated household variable (h) and the cumulated wealth variable (w) (both with maximal value normalized to unity). For this, we assume that the probabilities (ρ_k) represent a given fraction of households or population associated with mode k. Therefore, for the cumulated household variable, we add the probabilities (ρ_k) up to some

index value (m), and for the cumulated wealth variable, we add $(w_k/w_s)\rho_k$ in a similar way, where $w_k = E_k$ (wealth/energy value of agent/mode k) and $w_s = E = \sum_{l=0}^{N-1} w_l \rho_l$ (average wealth/energy over all agents/modes with probabilities (ρ_l)). More explicitly, we construct the Lorenz curve as the set of points $(h(m), w(m))$ for $m = 0, 1, \ldots, N$ with the partial sums of $w(m) = \sum_{k=0}^{m-1} w_k \rho_k / w_s$ and $h(m) = \sum_{k=0}^{m-1} \rho_k$ such that $0 \leq h, w \leq 1$. Here, the maximal values of h and w are $w(N) = h(N) = 1$, since $w_s = \sum_m w_m \rho_m$ and $\sum_m \rho_m = 1$. (Note that this procedures gives $N + 1$ data points for a spectrum with N modes due to the trivial initial value of $h(0) = w(0) = 0$). This procedure can be implemented directly for a given spectrum at a finite N value, provided we have first determined (for the given energy E) the chemical potential (μ) that fixes ρ_k by (5). In both Appendices A and B, we compute these partial sums analytically in the limit of $N \to \infty$ as integrals resulting in explicit expressions for the Lorenz curves ($w(h)$), as expressed by Equation (A6) for the RJS model and Equations (A14) and (A15) for the RJE model. However, these expressions still depend on the chemical potential, which is to be determined by the suitable implicit equation (for given values of E and a for the RJE model; see Appendices A and B for more details).

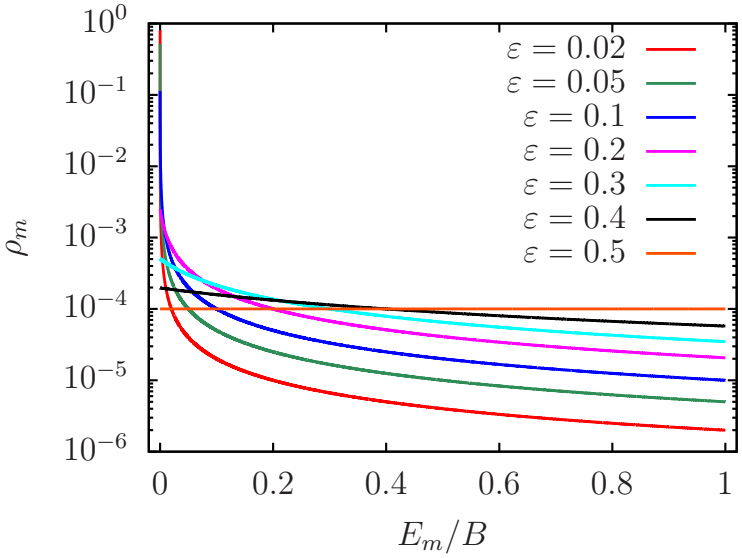


Figure 3. Dependence of the thermalized occupation probabilities ($\rho_m = T/(E_m - \mu) = (E - \mu)/[N(E_m - \mu)]$) on E_m/B for the RJS model ($E_m = m/N$, $N = 10{,}000$ and different values of ε).

Examples of Lorenz curves for the RJS and the RJE model (at $a = 4.5$) at various values of the rescaled average energy ($\varepsilon = E/B \approx E$; here, $B \approx 1$) are shown in Figure 4 (left or right panel for RJS or RJE with $a = 4.5$, respectively). Here, we show the Lorenz curves obtained by the analytical expressions of the appendix for the limit of $N \to \infty$, but we have verified that the curves for finite $N = 10^4$ are identical in terms of graphical precision, with an error similar to or less than 10^{-4}, which is illustrated in Figures A1 and A2.

For both models, the curves of Figure 4 show that at smaller values of ε (lower values of T), we have larger values of the Gini coefficient (G) closer to unity (stronger inequality). For the RJS model at the largest possible value of $\varepsilon = \varepsilon_C = 0.5$ (or, more precisely, slightly below ε_C to have a stable solution for μ), we have the simple expression pf $w = h^2$ with $G = 1/3$, which can be understood by the fact that this case corresponds to $T \to \infty$, with $\rho_l = 1/N$ =const. (see also the orange line at $\varepsilon = 0.5$ in Figure 3) such that $h(m) = m/N$ and $w(m) = \sum_{l=0}^{m-1} l/(\varepsilon_C N^2] \approx (m/N)^2$ (see also Equation (A8) and subsequent discussion in Appendix A).

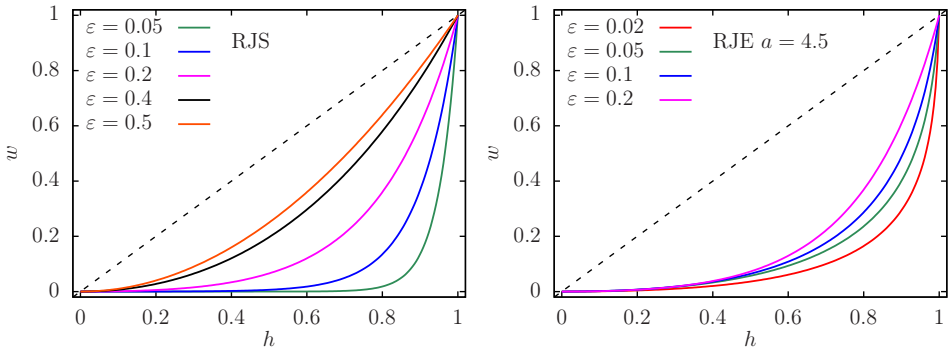


Figure 4. (**Left panel**): Lorenz curves for the RJS model for $\varepsilon = 0.05,\ 0.1,\ 0.2,\ 0.4,\ 0.5$ (bottom to top). The x-axis corresponds to the cumulated fraction of households (h), and the y-axis corresponds to the cumulated fraction of wealth (w). The dashed line is the line of perfect equipartition ($w = h$). The respective values of the Gini coefficients (G) for all curves are $G = 0.900,\ 0.800,\ 0.625,\ 0.407,\ 0.333$. **Right panel**: Lorenz curves for the RJE model at $a = 4.5$ for $\varepsilon = 0.02,\ 0.05,\ 0.1,\ 0.2$ (bottom to top) with respective Gini coefficients of $G = 0.798,\ 0.725,\ 0.678,\ 0.615$. Note that for these two cases, the critical value of ε for the transition of positive temperature (with $\mu < 0$) to negative temperature (with $\mu > B = 1$) is at $\varepsilon_C = 0.5$ (**left panel**) and $\varepsilon_C = 0.211$ (**right panel**) and that the RJS Lorenz curve at $\varepsilon = 0.5$ is given by the simple expression of $w = h^2$. In this figure, we use, for both RJS and RJE models, the continuous limit of $N \to \infty$, but the curves for finite $N = 10{,}000$ are identical on the basis of graphical precision (differences typically below 10^{-4}; see also Figures A1 and A2). We recall that the RJS model is a special case of the RJE model at $a = 0$.

For the continuous RJS model and small $\varepsilon \leq 0.2$, we also have (for $N \to \infty$) the very simple, quite accurate approximations of $w(h) \approx e^{(h-1)/\varepsilon}$ and $G \approx 1 - 2\varepsilon$, combined with $\mu \approx -e^{-1/\varepsilon} \ll \varepsilon$ (see Appendix A and, in particular, Figure A1 for more details on this).

The parameter choice of $a = 4.5$ for the RJE Lorenz curves in the right panel of Figure 4 corresponds to a typical value, which gives a good fit with real data (see next section). For this case, the critical energy ($\varepsilon_C = 1/a - 1/(e^a - 1) \approx 0.211$) for the transition to negative temperatures is significantly lower, as for the RJS case, since here, there are more levels at smaller energies, resulting in a reduced energy center of mass.

To compare the results of the RJS and the RJE model with real Lorenz curves, we apply the following procedure. First, for both cases, we fix the rescaled energy ($\varepsilon = E/B$) by the condition that the Gini coefficient (G) for the RJS/RJE model is equal to its value of the real Lorenz curve. This is a simple and efficient choice that is possible because G is a decreasing function with respect to increasing values of ε, as can be seen in both panels of Figure 4. Concerning the a parameter of the RJE model, we minimize a certain functional that measures the geometrical (orthogonal) curve distance between both curves (under the constraint that for each value of a, the value of ε is recomputed by the condition of identical Gini coefficients between the two curves). We do not enter into more details of this procedure, which is more complicated than a simple fit and that requires three levels of iterations to determine μ, ε and a. We have implemented this procedure for both cases of finite N and the continuous limit of $N \to \infty$ with very similar results.

We have also observed that modest variations of a, e.g., from $a = 4.5$ to $a = 4.4$, provide only very minimal modifications of the resulting Lorenz curves, provided that the value of ε is recalculated to match the initial Gini coefficient. We have also tested different variants of this procedure where the curve distance is minimized on a logarithmic scale or for the Pareto curve on a double logarithmic scale (see next subsection), which provide sometimes quite different solutions for the a parameter. However, for simplicity, we do not enter into more details on this, and all results for optimal a values for the RJE model with respect to some real data presented in this work were obtained for the Lorenz curve on a normal scale.

2.3. RJ Implications for the Pareto Curve

The Lorenz curve describes the global wealth distribution, and it focuses mostly on the main bulk of the whole population, e.g., for the world population [7,8], the typical value of $w(0.5) \approx 0.02$ shows that about 50% of the lower part of the population owns only 2% of the whole wealth. However, in economy studies of inequality, there is also a significant interest in the properties of the small oligarchic fraction of the population (usually about a few percent) that owns a huge amount of the total wealth (about 50%; see, e.g., [47]). A special analysis of this small part of the Lorenz curve is usually described by the Pareto curve [48], which assumes a power-law distribution decay of owners with high wealth (see, e.g., [6]).

For practical analysis, it is therefore also useful to consider the cumulative distribution function (CDF, $C(w_m)$) which gives the fraction of households (companies, people, countries, etc.) with wealth larger than w_m and to show it in a double logarithmic representation such that eventual power-law tails are adequately visible. Mathematically, the case of the expression Pareto distribution corresponds to the special form of $C(w_m) = 1$ for $w_m > w_0$ and $C(w_m) = (w_0/w_m)^{-\alpha}$ with two parameters: $w_0 > 0$ and (typically) $\alpha > 1$. In our work, we simply use the notation of *Pareto distribution* for the CDF $C(w_m)$ for other more general cases where there is not (necessarily) a simple power law, e.g., the cases of the RJS and RJE, where it is possible to compute this function either numerically for a finite N or analytically in the limit of $N \to \infty$.

We mention that one can also study the usual probability density function (PDF) in w_m defined by $p(w_m) = -C'(w_m)$ such that $p(w_m)\, dw_m = C(w_m) - C(w_m + dw_m)$ is the fraction of households with wealth in the interval of $[w_m, w_m + dw_m]$. However, in this work, we do not use the PDF and focus more on the CDF, also called the Pareto curve (together with the Lorenz curve).

From $C(w_m)$, one can compute the Lorenz curve ($w(h)$) in the following way: first, one defines the cumulated household quantity ($h(w_m) = 1 - C(w_m)$, with $0 \le h \le 1$), which corresponds to the fraction of (poorest) households that each has an individual household wealth of less than w_m. Then, one expresses $w_m = w_m(h)$ as a function of h and computes the integrated (and rescaled) cumulated wealth by $w(h) = W(h)/W(1)$ with $W(h) = \int_0^h w_m(\tilde{h})\, d\tilde{h}$ such that $w(0) = 0$ and $w(1) = 1$.

For example, for the exponential Boltzmann–Gibbs (BG) distribution at temperature $T > 0$, one has the following:

$$C_{\mathrm{BG}}(w_m) = e^{-w_m/T} \quad \Rightarrow \quad h = 1 - e^{-w_m/T} \quad \Rightarrow \quad w_m(h) = -T \ln(1-h) \quad \Rightarrow$$
$$W(h) = -T \int_0^h \ln(1-\tilde{h})\, d\tilde{h} = T[(1-h)\ln(1-h) + h],$$

which gives the Lorenz curve, i.e.,

$$w_{\mathrm{BG}}(h) = (1-h)\ln(1-h) + h\,. \tag{7}$$

This result was previously obtained in Ref. [6]. It respects the limiting cases of $w(0) = 0$ and $w(h) \to 1$ for $h \to 1$, and it no longer depends on T, i.e., the BG-Lorenz curve has no parameter. In particular, it has a fixed value for the Gini coefficient, which can be directly computed from (7) as $G = 1 - 2\int_0^1 w(h)dh = \frac{1}{2}$. Such a value is rather high (in comparison with typical real data), with a low degree of inequality. On the other hand, the derivative ($w'(h)$) diverges (logarithmically) for $h \to 1$, which is a manifestation of the fact that this model does not have a finite limit for w_m, which can take arbitrarily large values but with exponentially small probabilities such that the cumulated wealth stays finite. For real data, the RJS and RJE models have a finite limit of $w_m \le w_{\max}$ such that $w'(1)$ may be large but

is still finite (we typically apply a rescaling of units such that $w_{\max} = 1$). Furthermore, in real data, we typically have larger Gini coefficients of $G \sim 0.7$–0.9 or even $G \approx 0.95$ for some cases of the stock market or bitcoin (see below). Globally, the Lorenz curve and $C_{\rm BG}(w)$ for the BG model fit real data very poorly (see next section for two examples). In [6], the fact that the BG distribution always has $G = 0.5$, which is very different from real situations, was masked by the manual introduction of a complementary (power law) Pareto distribution at high wealth that gave a variation of G depending on a subjective fraction of the Pareto tail.

We also point out another important difference between the BG description [6] and the RJ model. Thus, for a gas of atoms, the BG distribution ($\rho_m \sim \exp(-E_m/T)$) describes fluctuations of kinetic energy of atoms (E_m), while the average steady-state energy of each atom is the same, i.e., $\langle E_m \rangle = 3T/2$ (in a 3D geometry). In contrast to this, the RJ distribution (1) gives already steady-state thermally averaged probabilities for given modes (m) that are more stable.

For the RJ distribution (1), the construction of the Pareto curve (at finite N) is straightforward according to the identification $of C(w_m) = \sum_{k=m}^{N-1} \rho_k$ (corresponding to $1 - h(m)$) and $w_m = E_m/E_{N-1}$ if we fix $w_{\max} = 1$. In Appendix B.6, we also compute the Pareto distribution analytically for the RJE model in the continuous limit of $N \to \infty$, which gives the precise expression (A32), together with the RJS limit (A33) obtained for $a \to 0$. Here, we only mention the nice simplified form, i.e.,

$$C_{\rm RJE}(w_m) \approx \frac{\varepsilon - \mu}{a}\left(\frac{1}{w_m} - 1\right), \tag{8}$$

which is typically valid for rather large values of a (e.g., $a > 7$); small values of ε (with $G \sim 0.8$–0.95); and the interval of $w_m \in [w_{\min}, 1]$, where $w_{\min} \ll 1$ is some small value (see the Appendix B for more details). If we exclude from this interval values close to unity, i.e., for $w_{\min} < w_m \ll 1$, the above expression becomes even a simple power law ($C_{\rm RJE}(w_m) \approx C_2 w^{-1}$) with an exponent of -1 and constant of $C_2 = (\varepsilon - \mu)/a$. However, we will see that this simple power law is only visible for cases with quite large values of a and small values of ε, where we have a significant interval for its validity.

3. WTH for Lorenz Curves of Countries and the World

In this Section, we compare the WTH theory, based on the RJS and RJE models, with the real Lorenz and Pareto curves of wealth inequality for households of countries and the whole world.

In Figure 5 (left panel), we show the Lorenz curve for wealth of households of the whole world in 2021. This curve is obtained from the data presented in [8] (from the front page of this website with interpolated cell data and best possible precision). For this data, the Gini coefficient is rather high, at $G = 0.843$. The Lorenz curve from the RJS model with the same G value clearly shows the presence of RJ condensation corresponding to the phase of poor households when 50% owns only 0.17% of total wealth, while according to [8], this fraction is 2%. However, even if the RJS model clearly captures the existence of condensate of poor owners, its shape differs from the real Lorenz curve obtained from data of [8]. Therefore, we also show the Lorenz curve for the RJE model with fit parameters of ε and a, which yields a curve very close to the real data of [8]. The left panel also shows the Lorenz curve from the BG theory [6], which is very different from the real data.

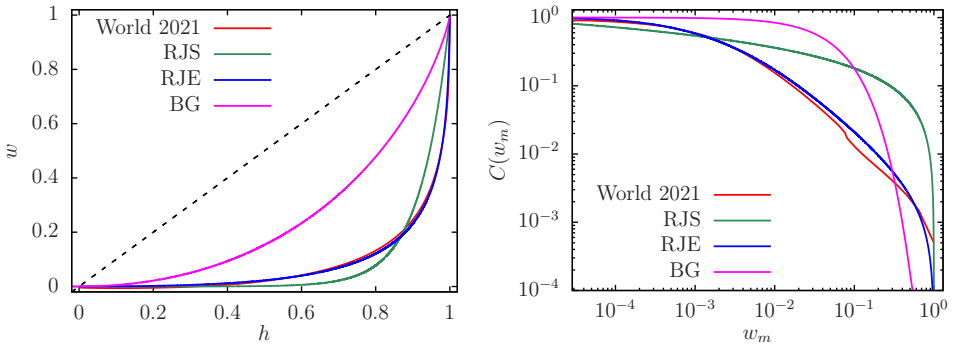


Figure 5. (**Left panel**): Lorenz curve of cumulated wealth distribution (w) vs. cumulated fraction of households h for the whole world in 2021 with a Gini coefficient of $G = 0.843$ (red curve with data taken from [8]), for the RJS model at $\varepsilon = 0.0784$ (green), for the RJE model at $a = 4.74, \varepsilon = 0.0113$ (blue) and for the BG model (pink) using expression (7), which is obtained in [6] and does not depend on T. The dashed black line shows the line of perfect equipartition ($w = h$). (**Right panel**): Pareto probability ($C(w_m)$) versus individual rescaled wealth (w_m) for the same cases and parameters as in the **left panel**. Here, for the BG model, $C_{\rm BG}(w_m) = e^{-w_m/T}$ depends on T and the shown pink curve corresponds to $T = 0.0574$ obtained by the fit of the $-w_m/T$ function with $\ln(C(w_m))$ for the World data. The values of ε for the RJS and RJE models are obtained from the condition that the corresponding Lorenz curves of these models have the same Gini coefficient as the World data, i.e., of $G = 0.843$. For the RJE model, the a parameter is determined by minimizing the geometric curve distance from the World Lorenz curve at a fixed G. Here, for both RJS and RJE models, we use the continuous limit of $N \to \infty$, but the curves for finite $N = 10{,}000$ are identical on the basis of graphical precision (differences typically below 10^{-4}) and provide very close values for ε and a.

In the right panel of Figure 5, we show the Pareto curve ($C(w_m)$) for the real Lorenz data [8] of the left panel. The data clearly shows that the BG theory does not work at all. Here, the BG curve still depends on the BG temperature, with a certain value of $T = 0.054$ used in Figure 5, although other values (using different fit procedures) are not better.

The RJS model describes only high values ($0.4 < C(w_m) \leq 1$) corresponding to small values of cumulated wealth (w) of poor households (h) (see left panel); it fails to describe households with high wealth. Indeed, the RJS model captures the condensation of households with low wealth, but it is not well suited for a description of rich households. However, the RJE model with an optimal parameter of $a = 4.74$ describes the Pareto curve well, including the oligarchic phase with very high wealth up to the very low Pareto probability with $C(w_m) \approx 7 \times 10^{-4}$. We point out that the Pareto curve shows a certain curvature and cannot be described by a simple power-law tail, as is usually expected (see, e.g., [6]). For the RJE model, the simplified analytical expression (8) agrees with the precise blue curve (and quite well with the red data curve) for $w \geq w_{\rm min} \approx 0.04$. Here, we theoretically have a power law with an exponent of -1 for the very short interval of $w \in [0.04, 0.1]$, which is roughly the slope of the blue curve in this interval (in double logarithmic representation), although globally, this interval is simply too small to claim power-law behavior for this case.

In Figure 6,we also show the Lorenz and Pareto curves for USA in 2019 taken from [49]. As for the case of Figure 5 the BG theory does not work; the RJS model captures the presence of condensation of poor households but has rather visible deviations from the real data for the Lorenz curve and even more for the Pareto curve. The RJE model describes the Lorenz curve data and the Pareto data well for $C(w_m) > 0.01$. For $C(w_m) < 0.01$, there are visible deviations from real, data even if the qualitative decay trend is captured. Here, the analytical expression (8) agrees with the RJE blue curve for $w \geq w_{\rm min}$, with the same value of $w_{\rm min} \approx 0.04$ as for the World 2021 case, which is plausible, since the obtained fit values of a and ε are, indeed, very close for both cases.

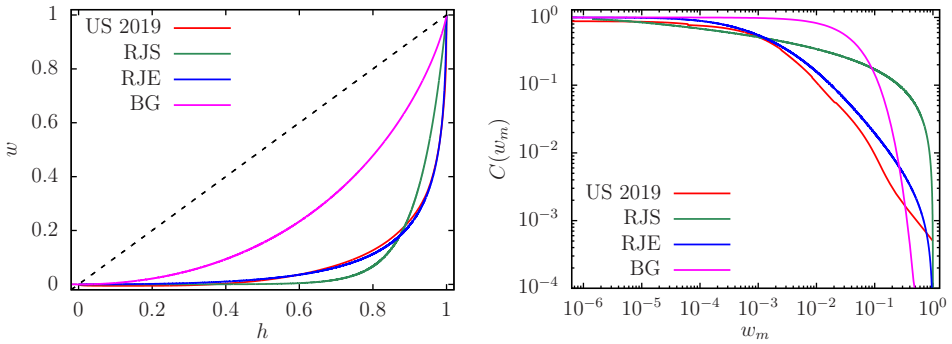


Figure 6. Same as in Figure 5 but for US 2019 with real data from [49]. The parameters are $G = 0.852$; $\varepsilon(RJS) = 0.0742$; $\varepsilon(RJE) = 0.0105$; $a = 4.72$; and, for the BG case in the **right panel**, $T = 0.0519$.

We should note that the real data available at [8,49] does not have sufficiently fine cells, so we used a smooth (rational) interpolation of data that is not very accurate at high wealth (w_m) values, which are especially important for the Pareto curve. Below, we discuss the properties of Pareto curves in more detail for the cases of stock exchange markets and bitcoin transactions, where the cell size is much smaller. We also describe the limiting continuous case when the cell size goes to zero (see Appendix B). Therefore, we use either the case with fine cell size or the continuous case. The fine cell size is conceptually rather clear and simple.

Finally, in Figure 7 we present the comparison of real Lorenz curves, taken from [50] for Germany and France in 2010, with the RJE model. It shows reasonable agreement between real data and the RJE theory, even if there are certain deviations of ≈ 0.014 (11%) (DE) and 0.032 (16%) (FR) in values of $w(h)$, e.g., at a given $h = 0.7$. In these cases, the Lorenz data are obtained with the best possible precision from the data figures of [50], combined with a smooth interpolation between raw data points extracted from these figures.

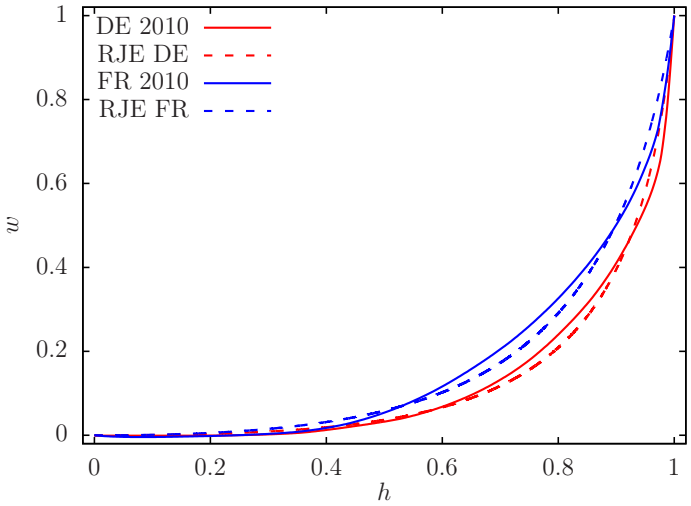


Figure 7. Lorenz curves for wealth of DE (full red curve) and FR (full blue curve) in 2010 using data of [50]. Dashed lines of the same color correspond to the Lorenz curves of the RJE model with optimal value of a and the same Gini coefficient as the reference data of either DE or FR. The parameters are $G = 0.750$, $a = 2.11$, $\varepsilon = 0.0682$ (DE) and $G = 0.676$, $a = 1.43$, $\varepsilon = 0.119$ (FR).

4. WTH for Lorenz Curves of GDP of Countries

Gross Domestic Product (GDP) is a monetary measure of the total market value of all final goods and services produced by a country during a year [51]. International organizations such as the United Nations (UN), International Monetary Fund (IMF) and World Bank (WB) report GDP values yearly for world countries and territories as, e.g.,

in [52] for recent years (with up to $N = 212$ countries). GDP country values for the years 1970–2023 are publicly available from the UN statistics division at [53], and we mainly use this data here. If we consider countries as independent players with equal rights according to the UN convention, then a striking feature of the GDP distribution of countries is a strong inequality when 50% of all countries own only 1% of the total GDP, while 10% (1%) of countries own 82% (44%) of the total GDP. (e.g., in 2023 [52,53]). It is interesting to note that this inequality of GDP distribution is very similar to the inequality of wealth distribution for households in countries (see numbers given above and [7–9]).

The GDP Lorenz curves for the years 1973, 1983, 1993, 2003, 2013, and 2023, obtained from UN data [53], are shown in Figure 8. In this time range of 50 years, the Lorenz curve remains remarkably stable, showing only small variations from year to year, despite the fact that the total world GDP changed enormously from 5.23×10^{12} in 1973 to 1.05×10^{14} USD in 2023 and the total number of countries and territories changed from $N = 187$ to $N = 212$ during this period (the list of all countries is available at [52,53]). The stability of the Lorenz curve confirms an adiabatic variation of the evolution of world GDP and the approximate conservation of the two integrals of motion.

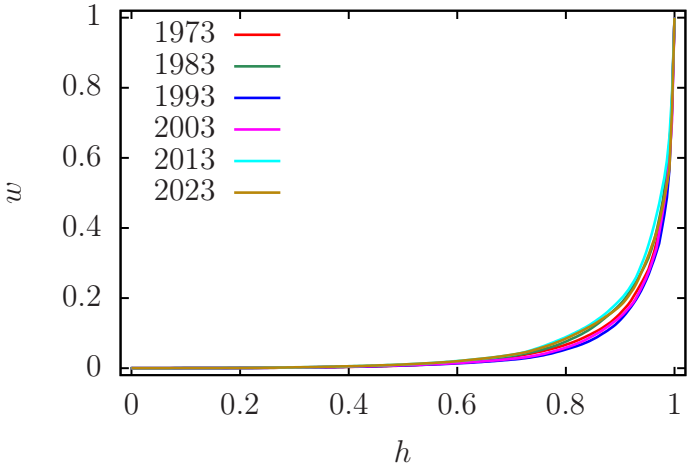


Figure 8. Lorenz curves of GDP for countries from UN data [53] for 6 years between 1973 and 2023. The x-axis corresponds the cumulated fraction of households/countries (h), and the y-axis corresponds to the cumulated fraction of wealth/GDP (w).

In Figure 9, we compare the GDP Lorenz curves of 1973 and 2023 with the WTH theory within the RJS and RJE models. The Lorenz curves for 1973 and 2023 are rather close to each other; thus, the parameters of the RJS and RJE models are also close for these 2 years (the same is valid for the other 4 years shown in Figure 8). On a scale of 50 years, the system parameters have only modest variations in the ranges: $0.871 \leq G \leq 0.904$; $0.0479 \leq \varepsilon(RJS) \leq 0.0646$; $0.0078 \leq \varepsilon(RJE) \leq 0.0157$; $3.622 \leq a \leq 4.31$. The RJS model describes the global behavior of Lorenz curves well but has visible deviations, while the RJE model gives almost perfect agreement with real data.

Of course, one can express a criticism, saying that a fit of a monotonic curve with two parameters (as for the RJE curve) may give rather good agreement with the a parameter, influencing the form of the spectrum (E_m) and the other parameter (ε), giving the rescaled energy. However, in our opinion, the most important point is not the almost perfect agreement of two curves of real data and the RJE model (even if it is useful to have it) but the physical origin of RJ condensation that naturally explains the appearance of the phase of high poverty and the oligarchic phase. The physical reason for RJ condensation is a small rescaled value of total system energy ($\varepsilon = E/B \sim 0.01 \ll 1$).

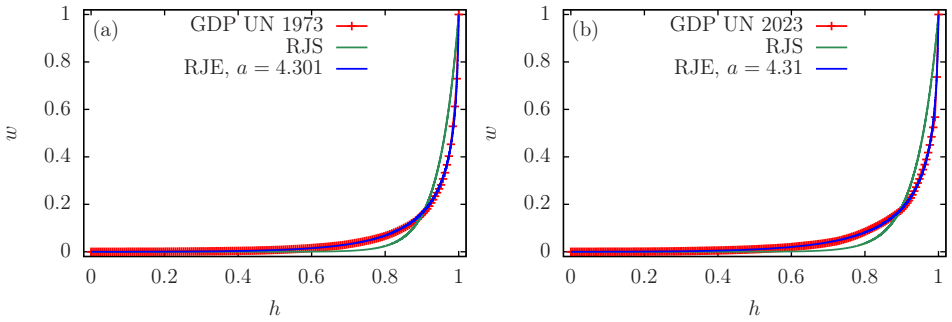


Figure 9. Panel (**a**): Lorenz curve for the year 1973 from UN data [53], shown by the red curve (with + symbols), with a Gini coefficient of $G = 0.892$; WTH theory with RJS model with $\varepsilon(RJS) = 0.0538$ at the same G (green curve); RJE model results are shown with a blue curve at $\varepsilon(RJE) = 0.00888$, $a = 4.301$; panel (**b**) shows, in the same style, data for the year 2023 with $G = 0.88$ and $\varepsilon(RJS) = 0.0601$ for the RJS model and $\varepsilon(RJE) = 0.01$ and $a = 4.31$ for the RJE model. The T and μ parameters for the RJS and RJE models for the year 2023 at $N = 212$ are given in the text.

We give the approximate values of system parameters B, T, and μ for the two cases of the RJS and RJE models for the UN data for 2023 in Figure 9b. For this year, we have $N = 212$ countries and territories, with the total world GDP being $E \approx 100$ trillion USD $= 10^{14}$ USD. For the subsequent discussion, we consider the RJS and RJE models at the same value of $N^{\mathrm{RJS/RJE}} = 212$ using the parameter values for ε and a of Figure 9b (the curves in this figure correspond to $N^{\mathrm{RJS/RJE}} = 10{,}000$). For the RJS model at $\varepsilon(RJS) = E/B = 0.0601$, this gives $B = E/\varepsilon \approx 1670$ trillion USD with a spacing between levels of $\Delta(RJS) = E_{m+1} - E_m = B/N \approx 7.9$ trillion USD. The solution of the two equations for the two conserved integrals, i.e., $\sum_{m=0}^{N-1} E_m \rho_m = E$ and $\sum_{m=0}^{N-1} \rho_m = 1$ with $\rho_m = T/(E_m - \mu) = (E - \mu)/[N(E_m - \mu)]$, gives $\mu = -0.74$ trillion USD and $T = (E - \mu)/N \approx E/N \approx 0.47$ trillion USD $\ll \Delta$, and the probability of the ground state is $\rho_0 = -T/\mu \approx 0.64$, indicating a rather strong RJ condensation.

For the RJE model, we have $\mu = -1.57$ trillion USD, $T \approx E/N \approx 0.47$ trillion USD, and $\rho_0 = -T/\mu \approx 0.30$. Here, the initial level spacing (at $m \ll N = 212$ and using $a = 4.31$) is $\Delta(RJE) = C/N = Ba/[N(e^a - 1)] \approx B(RJE)/(17N) = E/(17N\varepsilon(RJE)) \approx (6/17)\Delta(RJS) \approx 2.8$ trillion USD, which is still larger than T but smaller than $\Delta(RJS)$. Despite of the smaller value of $\varepsilon(RJE) = 0.01$, the effect of RJ condensation for the RJE model in comparison to the RJS case is a bit reduced but still clearly present, since the effect of the reduced value of ε (giving a factor of 6 for Δ) is more than compensated for by the the factor of $1/17$ from the exponential factor of $a/(e^a - 1) \approx 1/17$ resulting from the RJE model.

It is possible to decrease the fraction of the poverty phase by increasing the dimensionless system energy ($\varepsilon(RJE)$) as shown in Figure 10 for the RJE model for the year 2023 (at the same time, the structure of energies (E_m) is fixed with $a = 4.31 = const$ being independent of $\varepsilon(RJE)$). Indeed, the results of Figure 10 show that an increase in $\varepsilon(RJE)$ yields a significant reduction in the poverty phase (shown by blue color); however, this requires a quite strong boost of the $\varepsilon(RJE)$ parameter, which may not be an easy task. We note that here, as in [20] for the wealth of country households, we consider only cases with a positive temperature, which, for the RJE model at $a = 4.31$, corresponds to $\varepsilon(RJE) < \varepsilon_C = 0.218$.

Another wealth measure of a country can be expressed via the total Stock Exchange (SE) market capitalization of all domestic companies listed in the country SE (with World Bank data available from Wikipedia [54]). In recent years (2024–2025), this list has $N = 113$ countries, with a top total market cap of $M = 62{,}186$ billion USD for USA and the minimal value of $M = 0.388$ million USD for Mongolia. The ratio of Market Cap to GDP changes from country to country, being about 2.1 and 0.6 for USA and China, 0.8 for the UK, 1.3 for

France and 0.4 for Germany. Thus, the market cap represents a complementary country wealth measure in addition to GDP. The Lorenz curves for market cap data [54] are shown in Figure 11 in the same presentation style as in Figure 9 for GDP. As for GDP, data we find that the WTH describes the real data well: certain deviations are present for the RJS model, while the RJE model describes the data almost perfectly. The parameters of the RJS and RJE models are close to those of the GDP cases in Figure 9. The poverty phase that owns 2% of total Market Cap corresponds to 68% of countries, and 10% (1%) of countries own 82% (48%) of the total market cap. For the RJE model, the variations of the poverty and oligarchic phase with $\varepsilon(RJE)$ (for $a = 3.721$ and $\varepsilon_C = 0.244$) are shown in Figure 12, which is similar to the GDP case in Figure 10.

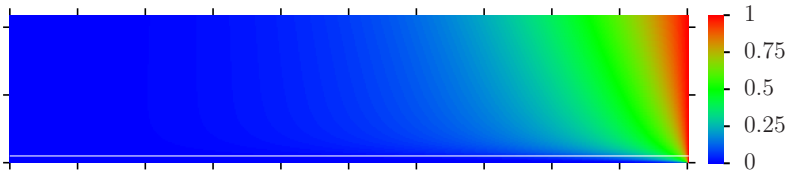


Figure 10. Color plot of wealth (w) from Lorenz curves of the RJE model at $a = 4.31$. The x-axis corresponds to the fraction of households ($h \in [0,1]$) , and the y-axis corresponds to the rescaled energy ($\varepsilon \in [0, \varepsilon_C]$, where $\varepsilon_C = 0.218$ is the critical value at which the transition from $T > 0$ to $T < 0$ appears). The ticks mark integer multiples of 0.1 for h and ε. The white line corresponds to $\varepsilon(RJE) = 0.01$ obtained from the fit of the RJE model using the GDP data of 2023 shown in Figure 9.

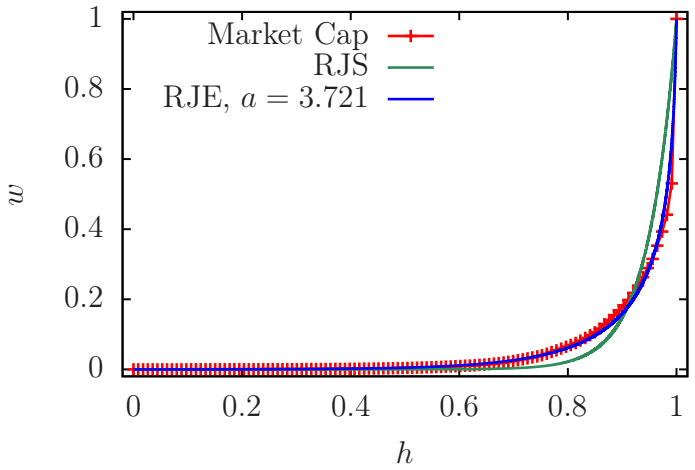


Figure 11. The Lorenz curve for SE market capitalization of $N = 113$ countries; data from [54]. The Lorenz curves are shown in the same style as in Figure 9. Here, $G = 0.895$, $\varepsilon(RJS) = 0.0525$ for the RJS model, and $\varepsilon(RJE) = 0.0119$, $a = 3.721$ for the RJE model.

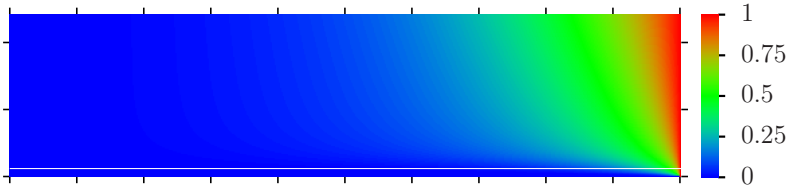


Figure 12. Same as Figure 10, with $a = 3.721$, $\varepsilon_C = 0.244$ and a white line at $\varepsilon(RJE) = 0.0119$ obtained from the fit of the RJE model using the SE Market Cap data shown in Figure 11.

The WTH approach describes the GDP distributions, wealth of country households [8], and distributions of market cap of SE companies presented in [20] well. Thus, for three types of players, the WTH theory explains existing inequality very well for wealth of individual persons, as well as the market capitalization of companies and the GDP distribution over countries. The number of persons for each such player is very different. But we argue

that the thermalization takes place for an individual player and not for individual persons that belong to a given player. This situation is similar to a case of a gas in a 3D box composed of different atoms: even if the masses are different for different sorts of atoms, the average kinetic energies of atoms are still the same, being equal to $3k_BT/2$, where k_B is the Boltzmann constant and T is the temperature. However, the atom square velocity is inversely proportional to atomic mass. Similarly, for the GDP per capita [55], the three top positions correspond to Monaco, Liechtenstein, and Luxembourg, which do not produce a significant influence on the world economy. Of course, for the GDP of countries, certain effects of a high or small country population may play some role, but we argue that this does not affect the RJ thermalization of the GDP distribution.

In Figure 13, we show the world map of RJE GDP values of countries computed from the RJE Lorenz curve of Figure 9b with optimal parameters of $a = 4.31$ and $\varepsilon = 0.01$ for the best fit with real UN GDP data for 2023 data from [51]. Qualitatively, we attribute to each of the 212 countries of the 2023 with an index of $m = 1, \ldots, 212$ ($m = 1$ for the country with minimal and $m = 212$ for the country with maximal GDP) the cumulated household interval of $[(m-1)dh, m\,dh]$, $dh = 1/212$ and take the wealth increase of $w_m^{(\mathrm{RJE})} = w(m\,dh) - w((m-1)dh)$ in this interval using the RJE curve ($w(h)$), which provides sum-normalized wealth values ($\sum_m w_m^{(\mathrm{RJE})} = w(1) - w(0) = 1$). Mathematically, we actually used the formula expressed as $w_m^{(\mathrm{RJE})} = CE_h((m-0.5)/212)$, where the constant ($C$) is determined by sum normalization and the $E_h(h)$ function is given by the analytic expression (A28) of Appendix B for the RJE energy expressed as a function of a cumulated household (h) computed for the limit of $N^{(\mathrm{RJE})} \to \infty$. This is a non-trivial function, since one has to take the RJE energy ($E_k = (e^{ak/N^{(\mathrm{RJE})}} - 1)/(e^a - 1)$) at the value of the rescaled index ($k/N^{(\mathrm{RJE})}$) that corresponds to a given household value ($h \in [0, 1]$; see Appendices B and C for details).

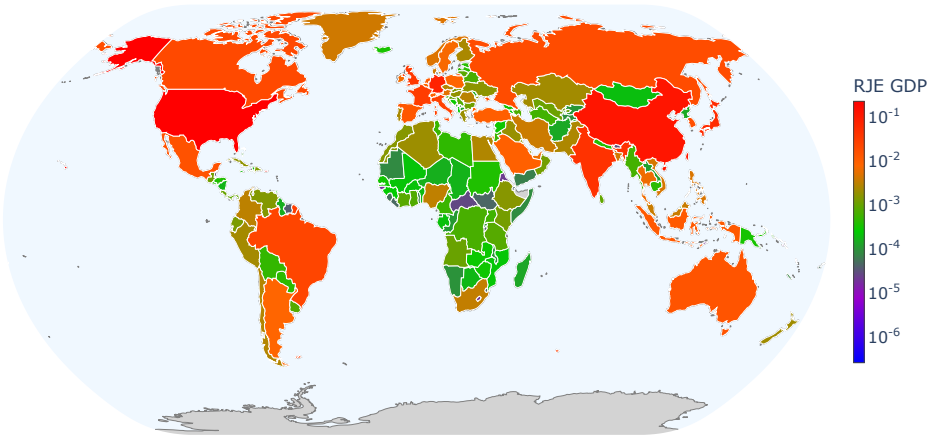


Figure 13. World map of RJE GDP values for 212 countries computed from the RJE Lorenz curve of Figure 9b at $a = 4.31$ and $\varepsilon = 0.01$, corresponding to the best RJE fit of real UN 2023 GDP data [53] (see text for details). The color values correspond to sum-normalized GDP values in logarithmic scale for the color bar.

A similar world map figure as in Figure 13 but for the real UN (sum-normalized) 2023 GDP data is shown Figure A3. The deviations between the two maps expressed by Δ_{GDP} are presented in the world map of (relative) differences in Figure A4. Furthermore, in Figure A5, we also show, on a logarithmic scale, the direct dependence of $w_m^{(\mathrm{RJE})}$ and the sum-normalized real data values (w_m) on the rescaled household index ($h = (m-0.5)/212$) for each country. Both curves cover six orders of magnitude for the rescaled GDP values and are very close, but for a few countries, there are significant deviations. Essentially,

$w_m^{(\mathrm{RJE})}$ represents a smoothed curve of the real values (w_m). In Appendix C, we also explain the link between the number of interacting agents in the RJE model and the cumulated number of households/countries. This number corresponds to the number of RJE energy modes (k) such that the associated cumulated household value for this mode index falls into the same cumulated household interval for a given country.

5. WTH Lorenz Curves for Stock Exchange Markets

In this section, we compare the RJE Lorenz and Pareto curves using real data of Market CAPitalization (MCAP) of companies on Hong Kong SE, Shanghai SE and London SE using publicly available data. According to the WTH concept, we assume that interactions between agents representing companies of a given SE lead to the RJ thermal distribution (1), which allows for the construction of Lorenz and Pareto curves as described in Section 2.

Thus, in Figure 14, we compare the Hong Kong SE MCAP data for 19 June 2025 with the RJE model with parameters obtained by a best fit (for the Lorenz curve). The RJE model describes not only the Lorenz curve very well but also the Pareto curve, which shows variations of $C(w_m)$ values for almost four orders of magnitude. The data clearly show that the Pareto curve has a curvature and cannot be described by a simple power-law decay with an exponent 1 or 2 that is usually argued to be valid in economy studies (see, e.g., [6]). In contrast to this algebraic decay of Pareto probability, we show that the decay is well described by the RJE model that reproduces the curved Pareto probability decay. The approximate RJE expression (8) agrees with the blue curve for $w_m \geq w_{\min} \approx 0.01$.

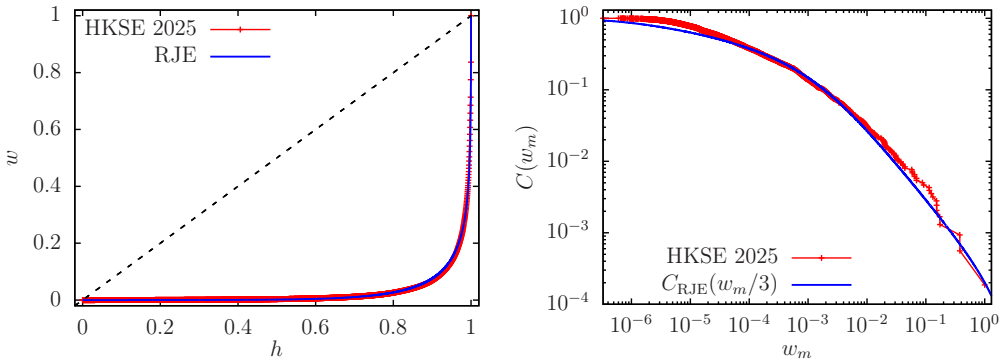


Figure 14. Lorenz (**left panel**) and Pareto (**right panel**) curves for MCAP of companies of the Hong Kong stock exchange (HKSE) on 19 June 2025 [56] (red curve/symbols) with $G = 0.947$ and the RJE curves (blue curve) with optimal values of $a = 7.04$ and $\varepsilon = 0.000706$ and a continuous limit of $N \to \infty$. The blue Pareto curve for the RJE model is shown with a rescaled argument ($C_{\mathrm{RJE}}(w_m/3)$), which excludes points at the very tail of $C(w_m)$ with small statistics (here, w_m is rescaled by the maximal company MCAP); the total number of companies is $N = 2683$.

In Figure 15, we show Lorenz and Pareto curves for the Shanghai SE on 18 November 2025 [57] in the same format as in Figure 14. The RJE model gives a satisfactory description of this data, even if deviations from real data are present for the Pareto curve. Here, the approximate RJE expression (8) agrees with the blue curve for $w_m \geq w_{\min} \approx 0.05$.

The London SE (LSE) provides an excellent detailed public archive [58] of MCAP data for the years spanning 1999 to 2024. There are data for each month and averaged data for each year. In Figure 16, we show the Lorenz curves for 6 selected years, with data for December of a given year and data averaged over the full year. There is a certain variation of curves, but globally, this variation is moderate. The Gini coefficient also has rather small variations during these years—in the range of $0.919 \leq G \leq 0.938$ (see data in Table 1). This Table represents Gini coefficients and other data for real Lorenz data studied in this work; we discuss this Table in detail a bit later.

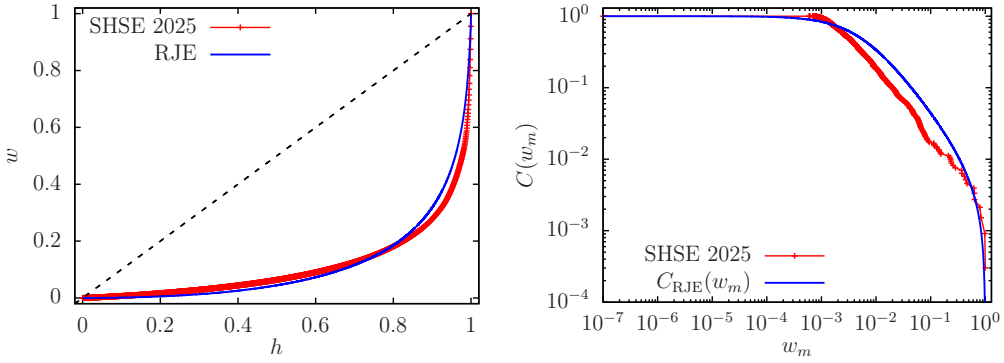


Figure 15. Lorenz (**left panel**) and Pareto (**right panel**) curves in the same format as Figure 14 for the MCAP of companies of the Shanghai SE (SHSE) on 18 November 2025 with $G = 0.778$ and data from [57] (red symbols, all visible) and the RJE model (blue curves) with optimal values of $a = 5.27$ and $\varepsilon = 0.0222$ and a continuous limit of $N \to \infty$. Here, the number of companies is $N = 1652$.

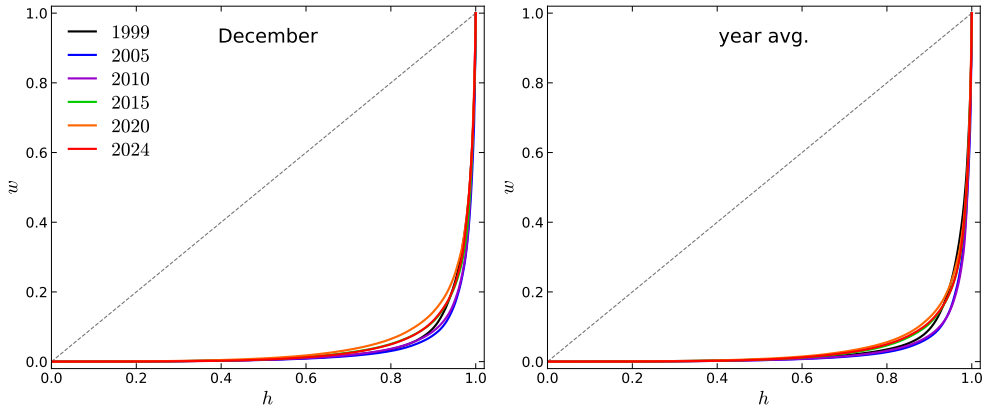


Figure 16. Lorenz curves of different years for the London Stock Exchange (LSE) in December (**left panel**) and averaged over the full year (**right panel**) for the same years as in the **left panel**.

The comparison of LSE data with the RJE model for the years of 1999 and 2024 are shown in Figure 17. For 2024, the Lorenz curve for real data (red) and the RJE curve (dashed green) are very close, even on a logarithmic scale for wealth (w); however, for Pareto curves, the deviations are adequately visible. For 1999, we have strong deviations for wealth values of $w < 0.01$, while the Pareto curves, in black and dashed blue, are closer to each other. Globally, we consider that the WTH theory gives a satisfactory description of the LSE data for these years. We recall that the RJE parameters of ε and a are obtained for the Lorenz curve data (in normal scale) and stress more moderate values of wealth, while the Pareto description stresses much more the region of very high wealth values. We also consider that the WTH description is not likely to be very exact for very small wealth values of $w < 0.01$, since the thermalization process can be very slow in the condensate phase. Furthermore, certain deviations present between raw data and the RJE curves on a logarithmic scale for very small values of w (Lorenz curves) or $C(w_m)$ (Pareto curves) are to be expected, since the fit procedures to compute the optimal RJE parameters (a and ε), by minimizing a certain functional for the geometric curve distance, are done for the Lorenz curves on a normal scale. Without going into much detail, we mention that modified fit procedures on a logarithmic scale (or for Pareto curves) may provide different values of a and ε such that the corresponding curves agree better on a logarithmic scale, whereas the quality of the fit in normal scale is reduced.

In Figure 18 we present the Pareto curves for the years and data shown in Figure 16 with Lorenz curves. This data provides size variations of approximately three to four orders

of magnitude for both quantities ($C(w_m)$ and w_m). We consider that these Pareto curves cannot be described by a simple algebraic decay in such a large interval.

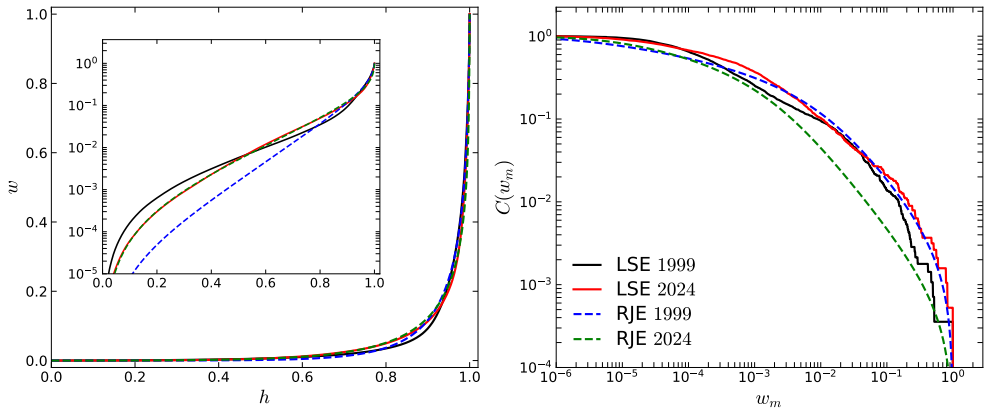


Figure 17. Year-averaged Lorenz curves for the years 1999 and 2024 of the LSE (**left panel**) and Pareto curves for the same data (**right panel**); LSE data are shown by full curves, and RJE model data are shown by dashed curves; here, $G = 0.920$ in 1999 with $N = 2807$ companies and $G = 0.917$ in 2024 with $N = 1900$; RJE parameters are $\varepsilon = 0.0087$ and $a = 3.79$ in 1999 and $\varepsilon = 0.0030$ and $a = 5.64$ in 2024; RJE curves are obtained in the limit of $N \to \infty$. The insert in the **left panel** shows data on a logarithmic scale for the y-axis.

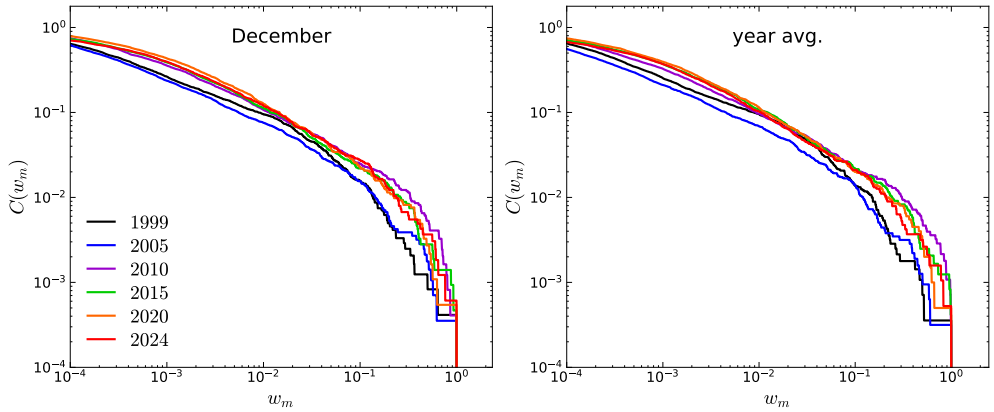


Figure 18. Pareto curves for the same LSE data as in Figure 16.

Globally, we consider that the WTH theory provides a good description of MCAP Lorenz and Pareto curves for the Hong Kong, Shanghai and London SEs.

We did not find public data for the New York SE, while S&P data is limited to only 500 companies representing only a quarter of all NYSE companies. For this reason, we do not discuss the NYSE here.

We note that stock markets can experience sharp changes when all market capitalization goes down. But as for an atomic gas, a sharp change in pressure can change the thermal equilibrium at a certain moment in time, after which collisions of atoms again bring the system to a state of thermal equilibrium. On a larger time scale, like a month or an year, like for London SE, such local fluctuations are averaged out. We point out that our results for Lorenz and Pareto curves of the London SE demonstrate its steady-state stability on a scale of a quarter of a century (see Figures 17 and 18), which, in our opinion, confirms the thermal stability of the SE. For the Hong Kong and Shanghai SEs, the Lorenz and Pareto curves are presented for one day of trade; these days were outside of any crises; thus, we consider that the data for these markets confirms the WTH description.

Table 1. Wealth inequality indicators for the World, the US, DE, and FR; the GDP of countries (UN data from 1973, 1993, and 2023), stock exchanges (Hong Kong (HKSE), Shanghai (SHSE), and London (LSE); year averages); the Bitcoin transaction network (quarterly data); and the World Trade Network (WTN). The columns correspond to system name; the Gini coefficient (G); and the share of total wealth held by the bottom 50%, the top 10%, and the top 1% of households/countries/companies/wallets.

System	Gini (G)	Bottom 50%	Top 10%	Top 1%
World and countries — annual average household wealth				
World 2021	0.842	2.0%	75.3%	37.3%
US 2019	0.852	1.5%	76.7%	37.4%
DE 2010	0.749	3.2%	59.0%	18.3%
FR 2010	0.676	5.4%	49.9%	11.7%
Gross domestic product — annual average country GDP (UN data)				
GDP UN 1973	0.892	0.7%	84.3%	37.2%
GDP UN 1993	0.904	0.8%	86.3%	44.3%
GDP UN 2023	0.880	1.0%	82.2%	43.8%
Stock Exchange — annual average market capitalization				
HKSE 2025	0.947	0.3%	93.2%	63.6%
SHSE 2025	0.778	6.4%	72.2%	38.8%
LSE 1999	0.920	0.6%	90.7%	40.9%
LSE 2005	0.938	0.4%	93.0%	50.7%
LSE 2010	0.937	0.4%	92.5%	51.0%
LSE 2015	0.919	0.6%	89.1%	46.2%
LSE 2020	0.909	0.7%	87.4%	44.7%
LSE 2024	0.917	0.5%	88.7%	45.8%
Bitcoin transaction network — wallet wealth (Q1 snapshots)				
Bitcoin 2011 Q1	0.887	1.6%	83.5%	54.5%
Bitcoin 2012 Q1	0.917	0.9%	87.5%	68.5%
Bitcoin 2013 Q1	0.944	0.5%	92.8%	65.8%
World Trade Network — country total trade (imports + exports)				
WTN 1965	0.770	3.6%	67.3%	12.9%
WTN 1975	0.802	2.3%	70.2%	16.2%
WTN 1985	0.794	2.1%	68.8%	17.2%
WTN 1995	0.832	1.2%	73.1%	17.3%
WTN 2005	0.845	1.0%	75.0%	19.8%
WTN 2014	0.801	1.7%	65.6%	18.0%

6. WTH Lorenz Curves for Bitcoin Transactions

In this Section, we present WTH results for Lorenz and Pareto curves of bitcoin transactions. The first Lorenz curves for bitcoin were shown in [59] (see Figure 15 there) on the bases of the transactions collected by Ivan Brugere for the period of 2009 to April 2013 and publicly available at [60]. An interested reader can find more information about bitcoin, e.g., in [61–64]. The transactions are perofmred between so called wallets [61]; in [59], it was shown that incoming and outgoing transactions between wallets yield almost the same Lorenz curves (see Figure 15 in [59]), so here, we present the Lorenz curves using the sum of incoming and outgoing transactions. More details about the properties of the bitcoin network for the above period are available in [59].

Here, we present Lorenz and Pareto curves for bitcoin transaction collected for the first quarters (Q1) of 2011 (2011Q1), 2012 (2012Q1), and 2013 (2013Q1). The Lorenz curves shown in Figure 19 match the associated RJE curves very well (with optimal fit parameters given in the caption). We note that these cases correspond to quite large values of $G \sim 0.9$–0.95 and $a \sim 7$–12, with very small values of $\varepsilon \sim 10^{-3}$ or smaller.

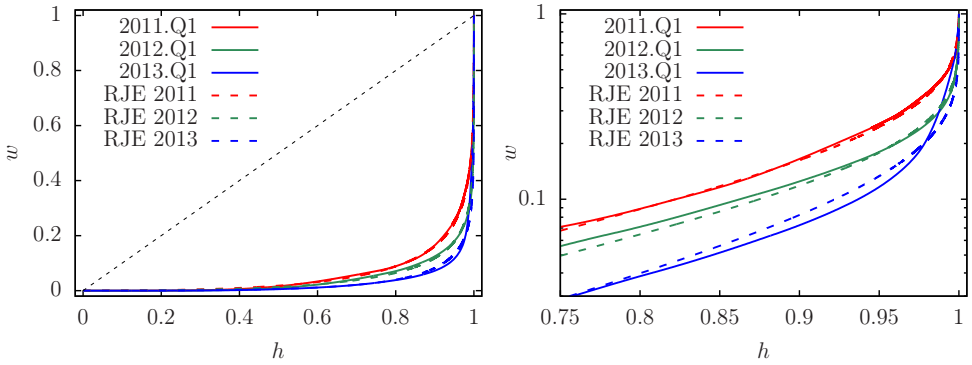


Figure 19. Comparison of the Lorenz curves for Bitcoin data in 2011Q1, 2012Q1, and 2013Q1 (full curves), along with the corresponding RJE curves with optimal fit parameters for each case (dashed curves). The respective Gini coefficients are $G = 0.887,\ 0.917,\ 0.944$, and the RJE model parameters are $\varepsilon = 1.30 \times 10^{-3},\ 1.05 \times 10^{-4},\ 2.64 \times 10^{-5}$ and $a = 7.61,\ 10.48,\ 11.43$; **left panel** shows all scales, and the **right panel** shows a zoom for rich wallets on a semi-logarithmic scale.

The comparison of real Pareto curves (with the datasets of Figure 19) and the curves of the RJE model (with the same parameters as in Figure 19) is shown in Figure 20. The variation range for the Pareto curve is seven orders of magnitude for $C((w_m)$ and eight orders of magnitude for w_m. There are significant fluctuations of the Pareto probability that are especially visible for the 2012Q1 and 2013Q1 datasets. However, the RJE model provides a satisfactory description of the global behavior in this huge range of variation of Pareto probability. We note that the tail of $C(w_m)$ corresponds to small transaction statistics (only a few events), and their exclusion significantly improves matching with the RJE Pareto curves (see right panel of Figure 20).

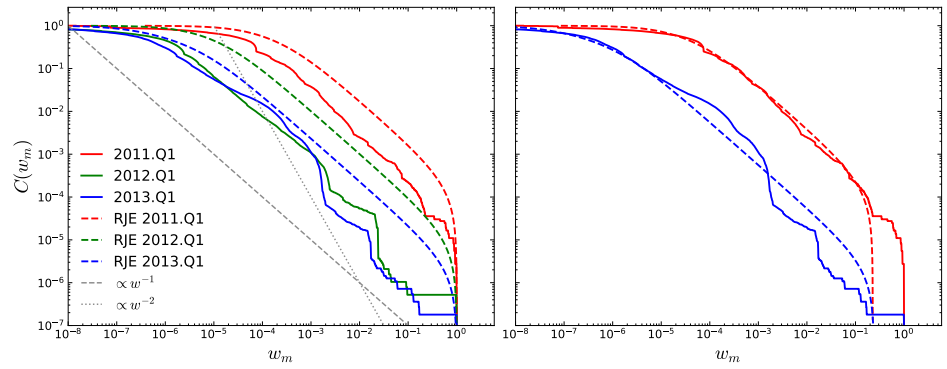


Figure 20. Pareto curves for the same Bitcoin data used in Figure 19 (full curves); RJE curves are shown by dashed lines; the **left panel** shows all cases (with w_m rescaled by its maximal value), and the **right panel** shows data and shifted RJE curves for the cases of 2011Q1 and 2013Q1, where the horizontal shift to the left excludes the contribution of $C(w_m)$ data, with very low transaction statistics at the extreme tail (Data from [60]). The black dashed and dotted straight lines in the **left panel** show the algebraic slopes of $C(w_m) \propto 1/w_m, 1/w_m^2$.

Due to the large values of a and small values of ε (with even smaller values of $|\mu|$), we are in a regime of the RJE model where the approximate expression (8) is valid over a very large interval of $w_m \in [w_{\min}, 1]$, e.g., with $w_{\min} \approx 3 \times 10^{-5}$ for the Bitcoin data of 2013.Q1 (see blue full and dashed lines). In the reduced interval of $w_m \in [w_{\min}, 0.1]$, we can neglect the constant term in (8), which gives the pure power-law behavior ($C(w_m) \approx C_2\, w_m^{-1}$) with an exponent of -1 and $C_2 \approx (\varepsilon - \mu)/a$ corresponding to a straight, dashed blue line (for this interval). For the other two cases of 2011.Q1 and 2012.Q1, we can also identify a significant interval where the same power law is valid (see regions where the red and green dashed lines are straight, with the exponent/slope being -1). However, for these two cases,

the interval is slighter smaller than for the case of 2013.Q1, with largest a and G values. We insist that in all cases, the power law does not extend to the full interval up to $w_{\max} = 1$, and here, the constant term in (8) is, indeed, important, since it implies $C(w_m = 1) = 0$ and a curved line in double logarithmic representation (for $w_m \in [0.1, 1]$).

Finally, in relation to the statistical description of bitcoin transactions, we note that there are recent works [65,66] where bitcoin statistics are discussed within the framework of the Bose–Einstein thermal distribution of bosonic particles based on the argument that bitcoins are non-distinguishable, like bosons. We find this idea somewhat strange, since there are no obvious quantum aspects associated with bitcoins. Therefore, their thermal distribution should be described by the RJ distribution (1), which is valid for classical mechanics and classical objects, which are very different from the quantum BE distribution (2). It is true that at high temperatures, the BE distribution is reduced to the RJ case, but at such temperatures, there is no RJ condensation (see our notes above about the works of Fröhlich [41,42]). The datasets studied in [65,66] are also significantly smaller than those considered here.

In the above figures with Pareto curves, we used a normalization of w_m values by the maximal w_m value (see, e.g., Figure 20). However, the maximal value of w_m is on the very tail of the distribution ($C(w_m)$) , where the statistical fluctuations are rather strong. It is also possible to normalize w_m not by the maximal but by its average value ($\langle w_m \rangle$) with reduced fluctuations. We show in the Supplementary Material that this normalization gives a more reliable description of real Pareto curves (see Supplementary Material Figures S1–S8).

7. WTH Lorenz Curves for World Trade UN Data

Here, we present the WTH description for the Lorenz curves obtained from the UN COMTRADE data of trade between world countries studied in [67,68] for the years spanning 1965 to 2014. During this period, the number of countries (N) varied from 86 in 1965 up to 158 in 2014 (the maximum of reporting countries was 169 in 2005). For this period, the sum of import and export for all these countries varied from 0.34 trillion USD up tp 36.83 trillion in 2014. As for bitcoin transactions, the Lorenz curves for import (incoming flow) and export (outgoing flow) are very close to each other; thus, we present the effective wealth (w_m) of a country as the sum of import and export.

The Lorenz curves for world trade are shown in Figure 21, and the Gini coefficients and other parameters of these curves are given in Table 1. We see that over 50 years, the Lorenz curves and related Gini coefficients remain rather stable, showing only moderate variations. This is similar to the case of GDP Lorenz curves in Figure 8. The comparison of the world trade Lorenz curve of 2014 with the RJE model is presented in the right panel of Figure 21. It shows good agreement between trade data and the RJE model, even on the logarithmic scale for cumulated wealth.

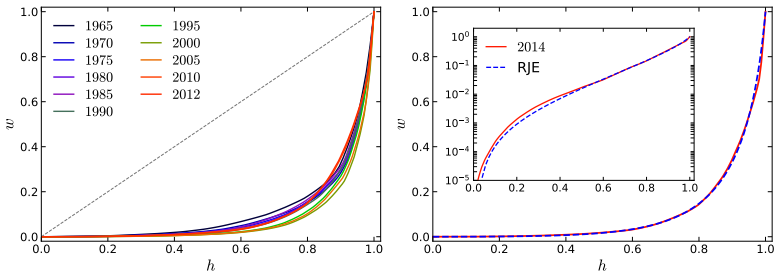


Figure 21. (**Left panel**): Lorenz curves for UN world trade data for different years (**right panel**): comparison of data for 2014 with the RJE Lorenz curve with parameters of $\varepsilon = 0.0623$ and $a = 1.556$; the Gini coefficient is $G = 0.801$ in 2014; other Gini values are given in Table 1. The insert in the **right panel** shows the Lorenz curves on a logarithmic scale for the y-axis.

8. Universality of the Thermodynamic Description of Inequality

Above, we presented analysis of real Lorenz curves for five types of wealth for five types of societies for households of countries and the world; GDP of world counties; market capitalization of companies on leading stock exchanges of Hong Kong, Shanghai, and London; bitcoin transactions between wallets; world trade between countries. The characteristics of Lorenz curves are presented in Table 1 in a style similar to that used in [8]. For all types of society, the Gini coefficient is above $G > 0.77$ (except for households in France and Germany). G is especially high for market capitalization and bitcoin transactions. For all five society types, we observe a huge poverty phase when 50% of households (or players or agents) own 2% of total wealth or less (with the exceptions of DE and FR in 2010 and Shanghai SE and WTN in 1965 and 1975). For almost all SE cases, we have even less than 1% (except for SHSE). At the same time, in the oligarchic phase, the top 10% owns more than 75% of total wealth, and the top 1% owns more than 37% of total wealth (with some exceptions for DE, FR and WTN). Moreover for the SE cases and bitcoins, in this phase, the top 10% owns almost 90% (with some exceptions). In our opinion, these results demonstrate universal features of wealth inequality in various types of societies and in the whole world.

Thermodynamics is a universal physical concept [1] that describes a variety of physical systems, including the black-body cosmic microwave background in the Universe described by the quantum BE distribution [2,3]. For classical systems, the BE distribution (2) is replaced by the RJ distribution (1), with temperature and chemical potential appearing due to energy and probability norm conservation. Above, we presented the RJ thermodynamic description for the wealth distributions in all five types of societies, showing that the WTH theory gives a good description of real Lorenz curves and Pareto curves (for households of countries, companies on SEs, and bitcoin wallets when the number of agents is large). Thus, we argue that the thermodynamic theory describes the wealth inequality in the world well. The most important feature of the RJ description is that within this concept, the condensation of poor households appears very naturally at low values of relative energy/the wealth of the system. We note that similar constraint-driven condensation also appears in a variety of physical systems (see, e.g., [44–46]).

Once more, we point out that RJ thermalization (1) appears due to certain interactions between agents of a considered system described by classical fields. This is a classical thermalization phenomenon without any quantum effects. Knowledge of the precise type of these interactions is not important. It is like in an atomic gas in a 3D black box, where almost any interactions between atoms lead to the emergence of the BG distribution of energy fluctuations of atoms, with an average kinetic energy of $3T/2$. Of course, the kinetic energy of an individual atom can fluctuate in time, but its average value is always equal to $3T/2$. In contrast to the BG case for the RJ thermalization, the average energy of mode m is described by (1), which we use in this work. We note that the energy fluctuations for excited energies are described by the BG distribution (see [28]), while for the condensate energies, the fluctuations are described by the Gumbel distribution (see [29]). The emergence of RJ thermalization and condensation from dynamical chaos of classical Newton equations of motions has been demonstrated in [20,26,28,29].

We stress once more that the RJ distribution (1) results from the conservation of system energy/wealth and the probability norm [1,27–29]. These average quantities can change slowly in time, corresponding to a certain adiabatic process when their average values are conserved. Indeed, typically, the GDP of a country changes from year to year only by a few percent, in favor of the conservation assumption for these quantities. The stability of the Lorenz curves for GDP, the London stock exchange and world trade on a scale of 25–50 years (see Figures 8, 16 and 21) also confirms this assumption. For bitcoin

transactions, we have data only for a relatively short time interval (see Figure 19), but even there, the variations of Lorenz curves are relatively moderate. Thus, we argue that the time variations of total energy and norm are adiabatic and that thermalization works locally in this adiabatic process.

9. Discussion and Conclusions

In this work, we described the thermodynamic properties of classical systems with two integrals of motion—namely, energy and the probability norm—where the RJ distribution has a condensation phase of low-energy states. We argue that energy can be associated with the wealth of agents in social systems, where, according to the WTH proposed in [20], the RJ thermalization naturally leads to the emergence of a huge poverty phase that owns only a few percent of total wealth and a tiny oligarchic phase that contains a huge amount of the total wealth. We presented real Lorenz curves of five types of societies (households of countries, GDP of countries, companies of stock exchanges, bitcoin wallets and world trade between countries) and demonstrated that the RJ description depicts these Lorenz curves well. The WTH RJ theory also gives a good description of Pareto curves for cases with many agents (households, companies, and wallets). RJ thermalization can appear due to nonlinear interactions between agents, leading to dynamical chaos, as shown in [20,26] for social networks with social stratification.

Here, we list the main assumptions on which the WTH approach is based: it is assumed that the analogy between energy levels represents the states of social and wealth stratification in a society well, and it is supposed that the interactions between these states are nonlinear and lead to a dynamical thermalization with conservation of two integrals of motion, i.e., total energy (wealth) and the probability norm. Such a thermalization is shown to take place in the social networks of society stratification models (see [20,26]). A specific form of density of such states is assumed (usually constant or decreasing with energy/wealth increase). In this frame, the distribution over these states is described by the RJ thermalization and condensation (1), which reproduce the real Lorenz curves well on a scale of 30–50 years for various countries and companies as described above. The RJ condensation gives a physical natural explanation of the emergence of poverty and oligarchic phases.

We note that it is possible to decrease the poverty phase via a reduction in wealth dispersion (B) in a society, which leads to an increase in relative system energy (ε) as shown in Figure 10. Such an action is reminiscent of the Zucman tax for high revenues (see, e.g., [47,69]). According the mathematical description of the RJ thermalization, such an action would, indeed, reduce the dispersion (B) and increase relative system energy (ε), thereby reducing wealth inequality. However, we leave a discussion of effects of such an action in real human society to economists and sociologists.

Supplementary Materials: The following supporting information can be downloaded at https://www.mdpi.com/article/10.3390/complexities2030020/s1, it contains Figures S1, S2, S3, S4, S5, S6, S7 and S8.

Author Contributions: Conceptualization, K.M.F., L.E. and D.L.S.; methodology, K.M.F., L.E. and D.L.S.; investigation, K.M.F., L.E. and D.L.S.; resources, K.M.F., L.E. and D.L.S.; writing—original draft preparation, K.M.F., L.E. and D.L.S.; writing—review and editing, K.M.F., L.E. and D.L.S. All authors have read and agreed to the published version of the manuscript.

Funding: The authors acknowledge support from a grant of the ANR France project NANOX N° ANR-17-EURE-0009 in the framework of the Programme Investissements d'Avenir (project MTDINA). This work was granted access to the HPC resources of CALMIP (Toulouse) under allocation 2026-P0110.

Institutional Review Board Statement: Not applicable.

Informed Consent Statement: Not applicable.

Data Availability Statement: The data presented in this study are available upon request from the corresponding author due to large amount of data.

Conflicts of Interest: The authors declare no conflicts of interest.

Appendix A. Analytical Results for the Continuous RJS Model

Appendix A.1. Continuous Limit and Chemical Potential

For the RJS and RJE models with finite ε, it is possible to obtain explicit formulas in the continuous limit of $N \to \infty$ by replacing the sums over m with integrals over a rescaled index variable ($t = m/N \in [0,1]$). In this section, we present some results on this for the RJS model, and the extension to the RJE model will be given in the next Appendix B.

For the RJS model, we have $E_m = m/N = t$, and in the following, we also use $\varepsilon = E$ (since $E_0 = 0$ and $B = (N-1)/N \to 1$ for $N \to \infty$). In the limit of $N \to \infty$, the implicit Equation (6) becomes

$$1 = (\varepsilon - \mu) \int_0^1 \frac{1}{t-\mu}\, dt = (\varepsilon - \mu) \ln\left(\frac{1-\mu}{-\mu}\right), \tag{A1}$$

which can be rewritten in the following form:

$$\mu = -(1-\mu) e^{-1/(\varepsilon-\mu)}\,. \tag{A2}$$

Both equations determine μ as a function of $\varepsilon \in [0,1]$. In the limit of a small ε, one can simply iterate Equation (A2) by inserting $\mu_0 = 0$ in the RHS, which gives $\mu_1 = -e^{-1/\varepsilon}$ on the LHS, which can be inserted in the RHS to obtain a better value of, e.g., μ_2. This procedure converges nicely for small ε, and for other values of ε, one can use standard techniques to solve these equations numerically and efficiently. For $\varepsilon \ll 1$, the first approximation of $(-\mu) \approx e^{-1/\varepsilon} \ll \varepsilon$ is already very good.

To understand the limit of $|\mu| \gg 1$, it is more useful to consider ε as a function of μ, which is determined by (A1). Expanding the logarithm in (A1) up to the third order in $1/\mu$, one finds that

$$\varepsilon \approx \frac{1}{2}\left(1 + \frac{1}{6\mu}\right) \to \frac{1}{2} \tag{A3}$$

for $|\mu| \to \infty$, which is expected from the curve of μ in Figure 1. The $1/\mu$ correction in (A3) will be useful below.

Appendix A.2. Lorenz Curve

As explained in the main part of this work, to compute the Lorenz curve, we have to compute a partial sum over $\rho_m = (E-\mu)/[N(E_m - \mu] \to (\varepsilon - \mu)/(t-\mu)\, dt$ (with $dt = 1/N$ and $t = E_m = m/N$) to obtain the household fraction (h) and over $(E_m/\varepsilon)\rho_m$ to obtain the wealth variable. Now, we replace these partial sums with integrals up to some arbitrary value of $s \in [0,1]$, which provides functions $h(s)$ and $w(s)$, allowing us to determine the Lorenz curve $w(h)$. These partial integrals are

$$h(s) = (\varepsilon - \mu) \int_0^s \frac{1}{t-\mu}\, dt = (\varepsilon - \mu) \ln\left(\frac{s-\mu}{-\mu}\right) \quad \Rightarrow \quad s(h) = (-\mu)\left(e^{h/(\varepsilon-\mu)} - 1\right) \tag{A4}$$

and

$$w(s) = \frac{\varepsilon-\mu}{\varepsilon}\int_0^s \frac{t}{t-\mu}\,dt = \frac{\varepsilon-\mu}{\varepsilon}\int_0^s \left(1+\frac{\mu}{t-\mu}\right)dt = \frac{\varepsilon-\mu}{\varepsilon}s + \frac{\mu}{\varepsilon}h(s)\,. \tag{A5}$$

Inserting the second expression of (A4) in (A5), we obtain the following analytical expressions for the Lorenz curve:

$$w(h) = \frac{-\mu}{\varepsilon}\Big((\varepsilon-\mu)\Big(e^{h/(\varepsilon-\mu)}-1\Big)-h\Big) = \frac{1-\mu}{\varepsilon}\,e^{-1/(\varepsilon-\mu)}\Big((\varepsilon-\mu)\Big(e^{h/(\varepsilon-\mu)}-1\Big)-h\Big)\,. \tag{A6}$$

Here, the second expression of (A6) is obtained by replacing the global factor (μ) with (A2), which gives a more convenient expression. Using (A2), one can verify that (A6) satisfies the conditions of $w(0) = 0$ and $w(1) = 1$.

The second expression (A6) allows us to take the limit of $\varepsilon \ll 1$ with $\mu \approx -e^{-1/\varepsilon} \ll \varepsilon$ such that for $\varepsilon \ll 1$, we have the simplified Lorenz curve (replacing $\mu = 0$ in (A6)):

$$w(h) \approx e^{-1/\varepsilon}\left(e^{h/\varepsilon}-1-\frac{h}{\varepsilon}\right) \approx e^{(h-1)/\varepsilon}\,. \tag{A7}$$

Here, both expressions are equivalent approximations for a small ε with $e^{-1/\varepsilon} \ll 1$. The first (second) expression does not exactly verify the condition for $w(1)$ (or $w(0)$). The second expression is very simple and numerically quite sufficient for $\varepsilon \leq 0.2$.

We have verified that both expressions (A6) coincide with the numerical data shown in the left panel of Figure 4 up to graphical precision, with an error below 2×10^{-4} and for all values of ε used in Figure 4. The approximate formulas (A7) are valid for $\varepsilon \leq 0.2$, with an error $\sim 10^{-2}$ for $\varepsilon = 0.2$ (and smaller errors for smaller values of ε). This can be seen in Figure A1, comparing the data for $\varepsilon = 0.1,\ 0.2,\ 0.3$ between the analytic expressions and the data for $N = 10{,}000$. Even for $\varepsilon = 0.3$, only a modest deviation of the approximate curve is visible, while here and in all other cases, the more precise expression (A6) matches the numerical data very closely.

Appendix A.3. Other Quantities

Using the analytical expressions for $w(h)$, one can compute several other quantities. For example, it is interesting to consider the second-order expansion in h for $|h/(\varepsilon-\mu)| \ll 1$, which gives

$$w(h) = \frac{(-\mu)}{2\varepsilon(\varepsilon-\mu)}\,h^2\,. \tag{A8}$$

We know that the limit of $|\mu| \to \infty$ corresponds to $\varepsilon \to 1/2$ and, in this case (A8), is valid for all $h \in [0,1]$. This gives the very simple formula of $w = h^2$ (which is also obvious from the fact that $\rho_m = 1/N = \text{const.}$ for $|\mu| \to \infty$ and the way the Lorenz curve is constructed from ρ_m).

It is also possible to compute the Gini coefficient:

$$G = 1-2\int_0^1 w(h)\,dh = 1+\frac{2\mu}{\varepsilon}\left[(\varepsilon-\mu)^2(e^{1/(\varepsilon-\mu)}-1)-(\varepsilon-\mu)-\frac{1}{2}\right] = 1-\frac{\mu}{\varepsilon}-2(\varepsilon-\mu)\,. \tag{A9}$$

Here, the last simpler expression (A9) was obtained by replacing the exponential term using the implicit equation of μ. The limit of $\varepsilon \ll 1$ with $\mu \approx -e^{-1/\varepsilon}$ gives $G \approx 1-2\varepsilon$, which matches the values of G given in the caption of Figure 4 well for $a = 0$ and $\varepsilon \leq 0.1$ (a rather close value for $\varepsilon = 0.2$). The other values are matched exactly by the more precise expression (A9). Furthermore, inserting the expression (A3) for a large $|\mu|$ in (A9), one

finds (confirms) that $G = 1/3$ for $\varepsilon = 1/2$ (here, it is necessary to keep the $1/\mu$ correction in (A3) to obtain the correct result for G).

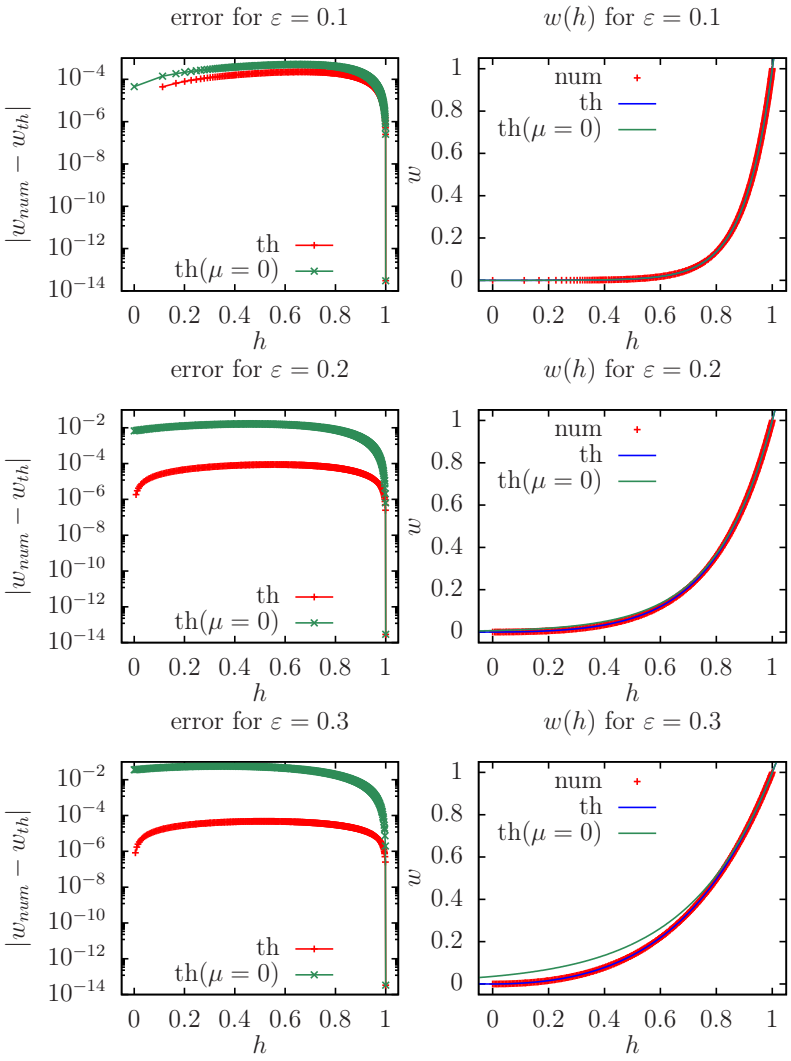


Figure A1. Comparison of Lorenz curves of the cumulated wealth fraction (w) versus cumulated household fraction (h) for the analytical model with the numerical data of the RJS model for finite $N = 10{,}000$ and for three key values of the rescaled energy ($\varepsilon = 0.1, 0.2, 0.3$ top to bottom). The (**left**) panels show the difference between the analytical model and numerical data, and the (**right**) panels directly show the curves (w) versus h for the numerical data (red lines and data points) and the analytical model. Blue lines (red data points in the left panel) correspond to the formula (A6) valid for all values of ε and using the appropriate value of the chemical potential (μ) determined by the implicit Equation (A1). Green lines (green data points in the left panel) correspond to the (second) approximate formula (A7) valid for small values of $\varepsilon \leq 0.2$. The discrete points of data in the top-right panel for $\varepsilon = 0.1$ at values close to $w = 0$ indicate finite values for $\rho_0 = 0.1129$, $\rho_0 + \rho_1 = 0.1660$, etc., due to RJ condensation.

Appendix A.4. General Discussion of the Continuous Limit

One might be concerned that the integral approximation is not very good for small values of μ (close to the singularity of the first term in (6)) and some finite but large values of N, such as $N = 10{,}000$. This is true, but the integral provides a modified logarithmic singularity, which also allows us to correctly mimic the condensation effect with correct probabilities. Therefore, even though the values of μ are modified for $\varepsilon \ll 1$ (but still $0 < -\mu \ll \varepsilon \ll 1$ for both models), the resulting probabilities (e.g., integrals or sums of ρ_m over some interval in $t = m/N$) are the same. The values of μ obtained by the continuous

analytical model match the curve shown in Figure 1 very well; of course, this figure does not allow for verification of whether $\mu \approx -e^{-1/\varepsilon}$ (continuous model) or $\mu \approx -\varepsilon/(N-1)$ (for the finite N model with discrete sums), which are both close to zero in the figure. In any case, we find that the analytical expressions given here (if μ is properly evaluated by its implicit Equation (A1) and if properly evaluated by avoiding numerical instabilities of some formulas in some special cases) match the numerical data with an error that scales with $1/N$.

Without going into details, we mention that we also considered a more refined version of the continuous model using a finite value of N and keeping the first singular term separate from the integral (which starts at $s = 1/N$ and not $s = 0$). In this case, we obtain a modified implicit equation of μ, which results in values of μ closer to the model of finite N, but the resulting physical quantities ($w(h)$ curves, Gini coefficients, etc.) are (numerically, with an error $< 10^{-4}$) the same as both the numerical data and the simple model. The resulting analytical expressions of the refined model are slightly modified (essentially replacing h with $h - \rho_0$ for $h \geq \rho_0$ in the formula of the Lorenz curve and using $w(h) = 0$ for $h < \rho_0$, where ρ_0 may now have a finite value). Note that the initial interval of $h \in [0, \rho_0[$ with exactly $w(h) = 0$ for the refined and discrete model translates to exponentially small values of $w(h) \approx h^2\, e^{-1/\varepsilon}/(2\varepsilon)$ for the simple analytical model (replacing $\mu \approx -e^{-1/\varepsilon}$ in (A8)).

Appendix B. Analytical Results for the Continuous RJE Model

Appendix B.1. Lorenz Curve

Here, we present an extension of the continuous limit of $N \to \infty$ to the RJE model. For this, we consider a real parameter (a) and the (rescaled) RJE spectrum ($E_m = E_s(m/N)$) with the smooth function ($E_s(s) = (e^{as} - 1)/D(a)$), where $s \in [0, 1]$ is a rescaled index variable and $D(a) = e^a - 1$ is a parameter dependent on a, which we will use in this appendix. In this way, the band width is, again, unity, i.e., $B = E_{N-1} \approx 1$ (and $B = 1$ exactly for $N \to \infty$). The limit of $a \to 0$ is well defined, and in this case, we simply recover $E_s(s) = s \quad \Rightarrow \quad E_m = m/N$, which is the RJS model, as a special case. Negative values of a are also possible but less relevant for comparison with real data. For the cases where the optimal RJE fit for some real data gives (modest) negative values for a, the simple RJS curve is typically already a very good fit.

Now, extending (A4), we have the cumulated household ($h(s)$) as a a function of the index variable (s) given by

$$h(s) = (\varepsilon - \mu) \int_0^s \frac{1}{E_s(t) - \mu}\, dt = (\varepsilon - \mu) \int_0^s \frac{D(a)}{e^{at} - b}\, dt = (\varepsilon - \mu) D(a) \int_0^s \frac{e^{-at}}{1 - be^{-at}}\, dt, \tag{A10}$$

where we have defined the quantity of $b = 1 + \mu D(a)$ for shorter notations and μ is the chemical potential (typically $\mu < 0$ for $T > 0$; its computation will be discussed in the next subsection). The last integral in (A10) can be computed in closed form and gives

$$h(s) = \frac{(\varepsilon - \mu) D(a)}{ab} \ln\left(\frac{1 - be^{-as}}{1 - b}\right). \tag{A11}$$

The integral for the cumulated wealth function ($w(s)$, depending on the index variable (s)) can be expressed in a similar way as (A5) for the RJS model:

$$w(s) = \frac{\varepsilon - \mu}{\varepsilon} \int_0^s \frac{E_s(t)}{E_s(t) - \mu}\, dt = \frac{\varepsilon - \mu}{\varepsilon} \int_0^s \left(1 + \frac{\mu}{E_s(t) - \mu}\right) dt = \frac{\varepsilon - \mu}{\varepsilon} s + \frac{\mu}{\varepsilon} h(s)\,. \tag{A12}$$

To obtain the Lorenz curve ($w(h)$) (cumulated wealth as a function of cumulated household), we need to use (A11) to express $s = s(h)$ as a function of h and insert the result for s in (A12). This calculation gives

$$e^{-as(h)} = \frac{1}{b}\left[1 - (1-b)\exp\left(\frac{abh}{D(a)(\varepsilon-\mu)}\right)\right] = 1 + \frac{\mu D(a)}{b}\left[\exp\left(\frac{abh}{D(a)(\varepsilon-\mu)}\right) - 1\right] \quad \Rightarrow \tag{A13}$$

$$s(h) = -\frac{1}{a}\ln\left\{1 + \frac{\mu D(a)}{b}\left[\exp\left(\frac{abh}{D(a)(\varepsilon-\mu)}\right) - 1\right]\right\} \quad , \quad b = 1 + \mu D(a)\,. \tag{A14}$$

Using this expression for $s(h)$, we have the closed formula for the Lorenz curve:

$$w(h) = \frac{\varepsilon-\mu}{\varepsilon}s(h) + \frac{\mu}{\varepsilon}h\,. \tag{A15}$$

We note that (A14) is written in a way that is numerically stable if the appropriate functions (`expm1(x)` for $\exp(x) - 1$ and `log1p(x)` for $\ln(1+x)$) are used, which are also accurate for $|x| \ll 1$ and typically available in any numerical computer library (C, Fortran, python, etc.). This point is important, since we want these expressions also to be useful in the limit of a small a or $-\mu$. Actually, taking the limit of $a \to 0$ (with $D(a) \to 0$ but $a/D(a) \to 1$), from (A14) and (A15), one obtained the first expression of (A6) for the RJS case, as it should be.

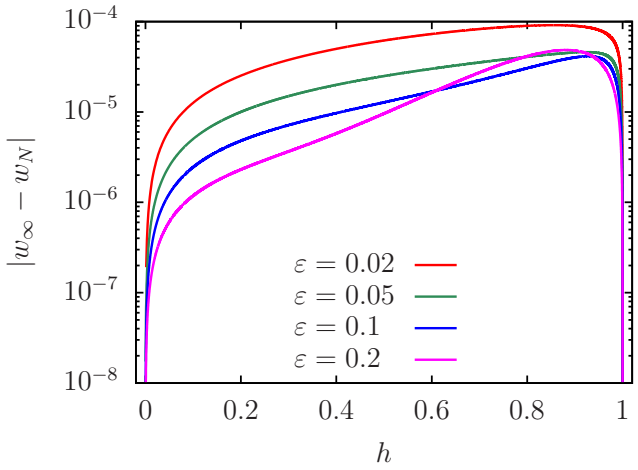


Figure A2. Difference of Lorenz curves for the RJE model at $a = 4.5$ between finite $N = 10{,}000$ and the continuous limit of $N \to \infty$ for the cases of the right panel of Figure 4. w_∞ is obtained by the combined expression of (A14) and (A15), while the curve for w_N is obtained for the finite $N = 10{,}000$ RJE spectrum as described in Section 2.2.

Figure A2 shows, for $a = 4.5$ and four ε values (cases of the right panel of Figure 4), the difference of the Lorenz curves obtained by the analytic expressions ((A14) and (A15)) with the finite $N = 10{,}000$ Lorenz curve constructed as explained in Section 2.2. The difference for all cases is clearly below 10^{-4}. (Concerning the computation of μ, see the next subsection.)

Appendix B.2. Implicit Computation of the Chemical Potential

The above results depend on the value of the chemical potential, which is determined by the condition of $h(s = 1) = 1$. Using (A11), this gives

$$1 = \frac{(\varepsilon-\mu)D(a)}{ab}\ln\left(\frac{1-(1+\mu D(a))e^{-a}}{-\mu D(a)}\right) = \frac{\varepsilon-\mu}{a(D^{-1}(a)+\mu)}\ln\left(\frac{e^{-a}(1-\mu)}{-\mu}\right). \tag{A16}$$

To solve this equation numerically, it is more convenient to reformulate it as follows:

$$\mu = -e^{-a}(1-\mu)\exp\left(-\frac{a(D^{-1}(a)+\mu)}{\varepsilon-\mu}\right) = -\frac{1}{\exp\left(\frac{a(D^{-1}(a)+\varepsilon)}{\varepsilon-\mu}\right)-1}\,. \tag{A17}$$

Both variants give a possible fixed-point iteration with a first approximation by inserting $\mu = 0$ in the r.h.s.:

$$\mu \approx -e^{-a}\exp\left(-\frac{aD^{-1}(a)}{\varepsilon}\right) \quad , \quad \varepsilon \ll 1. \tag{A18}$$

However, ut this fixed-point iteration has a very limited range of convergence that works only for extremely small values of $\varepsilon \ll 1$ (depending on a). However, the approximate value (A18) gives a good idea of the behavior of μ at small values of ε. For $a \to 0$, we recover $\mu \approx -e^{-1/\varepsilon}$ as already known from the RJS model. For a large a, there are two regimes of $\varepsilon \ll a/D(a)$ with $-\mu \sim e^{-(\ldots)/\varepsilon}$ and $a/D(a) \ll \varepsilon \ll 1$ with $-\mu \approx e^{-a} \ll 1$. Using (A18), it is possible to obtain more explicit formulas at $\varepsilon \ll 1$ for the Lorenz curve and other quantities (computed below), but due to complications associated with the two different regimes and the lack of space, we do not enter into more details on this point.

Concerning a careful numerical solution of (A17), it turns out that there is a technical complication, since (A17) also has a second non-physical solution i.e., $\mu = -D^{-1}(a)$ (which gives a singular result in (A14), since it has $b = 0$), and one must be careful to determine the other physical solution with $\mu \neq -D^{-1}(a)$. Fortunately, there is a nice numerical trick that consists of computing the solution of $0 = F_0(\mu) = (\mu - F_1(\mu))/(\mu + D^{-1}(a))$, where the denominator $\mu + D^{-1}(a)$ removes the non-physical solution. Here, $F_1(\mu)$ is either one of the expressions on the r.h.s. of (A17). In this case, the secant method (together with some pre-iterations to find two good start values with a sign change) allows us to efficiently find the zero of $F_0(\mu)$, which is, indeed, the physical solution. We mention that the non-physical solution is not a solution of the initial Equation (A16). However, the latter is numerically quite problematic to compute μ.

We also mention that one can solve approximately the (finite N) implicit Equation (6) in the limit of $|\mu| \to \infty$, which shows that $\mu < E_0 = 0$ (with $T > 0$) if $E < \sum_m E_m/N$ and $\mu > E_{N-1} = B$ (with $T < 0$) if $E > \sum_m E_m/N$. For the continuous RJE model, this means that the transition from $T > 0$ to $T < 0$ happens at the critical energy, i.e.,

$$\varepsilon_C = \frac{1}{N}\sum_{m=0}^{N-1} E_m \to \frac{1}{D(a)}\int_0^1 ds(e^{as}-1) = \frac{1}{a} - \frac{1}{e^a-1}, \tag{A19}$$

which has a limit of $\frac{1}{2}$ for $a \to 0$ and takes a value of $\varepsilon_C = 0.211$ for $a = 4.5$, as used in the data of Figures A2 and 4 (right panel).

The analytic results presented so far (and below in the next subsections) also apply to the case of negative temperature with $\varepsilon > \varepsilon_C$ and $\mu > 1$, eventually with some additional complications for the numerical stability (especially for $T < 0$ with $T \nearrow 0$ and $\mu \searrow B$). However, in this work, we do not insist on the case of $T < 0$; we typically assume $\varepsilon < \varepsilon_C$ with $T > 0$, and all optimal RJE fits presented here for real raw data correspond to this case.

Appendix B.3. Gini Coefficient

Using the analytic result for the Lorenz curve, we can also compute the Gini coefficient (G) as follows:

$$G = 1 - 2\int_0^1 w(h)dh = 1 - \frac{2}{a}\left(1-\frac{\mu}{\varepsilon}\right)F(x,y) - \frac{\mu}{\varepsilon} \tag{A20}$$

where

$$F(x,y) = -\int_0^1 dh \ln\left(\frac{1-xe^{yh}}{1-x}\right) \tag{A21}$$

with two auxiliary quantities

$$x = -\mu D(a) > 0 \quad \text{and} \quad y = \frac{a(1+\mu D(a))}{D(a)(\varepsilon-\mu)} = \frac{a(1-x)}{D(a)\varepsilon + x} \,. \tag{A22}$$

The integral (A21) can be computed in closed form using the *dilogarithm* defined by

$$\mathrm{Li}_2(z) = -\int_0^z \frac{\ln(1-t)}{t} dt = \sum_{n=0}^{\infty} \frac{z^n}{n^2} \,. \tag{A23}$$

Here, the first integral expression is well defined for $z \in]-\infty, 1]$ (maximal real interval where $\mathrm{Li}_2(z)$ has real values), and the power series converges for $|z| \leq 1$ (but with slow convergence if $|z| \to 1$). $\mathrm{Li}_2(z)$ can be numerically evaluated very efficiently by the power series for $|z| \leq \frac{1}{2}$ with very fast convergence, and for other arguments ($z \in]\frac{1}{2}, 1]$, $z \in [-1, -\frac{1}{2}[$ or $z \in]-\infty, -1[$), it is possible to use certain mathematical identities (e.g., reflection formula, etc.; see, for example the Wikipedia article on $\mathrm{Li}_2(z)$) to transform the argument inside an interval of nice convergence. In the mathematical standard literature, one also finds a different, very efficient expansion of $\mathrm{Li}_2(z) = \sum_{n=0}^{\infty} B_n(-\ln(1-z))^n/(n+1)!$ using the Bernoulli numbers (B_n) with faster convergence than the standard series given above (for $|z| \leq \frac{1}{2}$).

Using the dilogarithm (A23), for the $F(x,y)$ function, we obtain the following closed result:

$$F(x,y) = \ln(1-x) + \frac{1}{y}\Big(\mathrm{Li}_2(xe^y) - \mathrm{Li}_2(x)\Big) \quad \text{for} \quad x < 1 \quad , \tag{A24}$$

$$F(x,y) = -\frac{y}{2} + \ln\left(1-\frac{1}{x}\right) - \frac{1}{y}\left[\mathrm{Li}_2\left(\frac{1}{xe^y}\right) - \mathrm{Li}_2\left(\frac{1}{x}\right)\right] \quad \text{for} \quad x > 1 \quad , \tag{A25}$$

$$F(1,0) = \lim_{x\to 1} F(x,y(x)) = \frac{1}{A}(1-A)\,\ln(1-A) + 1 \quad , \quad A = \frac{a}{D(a)\varepsilon + 1} \quad \text{for} \quad x = 1 \quad . \tag{A26}$$

Together with (A20), these expressions provide a closed expression for the Gini coefficient (G). As for the Lorenz curve, we can perform the limit of $a \to 0$ (which corresponds to the case of $x \to 0$), which perfectly confirms the (first) expression in (A9) for the RJS model at $a = 0$. Note that the case of $x < 0$ is also possible if $a < 0$ and the above expression (A24) is also valid for this case (if $\mathrm{Li}_2(z)$ is correctly evaluated for $z < 0$).

We also verified the validity of the analytic result of G by a numerical computation of the integral of $w(h)$ over the interval of $h \in [0,1]$ for several values of a and ε. Note that standard numerical integration methods such as the Simpson or Romberg methods applied to $w(h)$ (using (A14) and (A15)) work better, i.e., provide more precise results at a given number of numerical support points, if the integration is done over the transformed variable ($u \in [0,1]$) with $h = 1 - u^4$ (and $dh = -4u^3\,du$) such that the difficult region of $h \to 1$ (where $w'(h)$ and $w''(h)$ are very large) has a higher density of support points.

We mention that the reliable and efficient computation of the Gini coefficient for the RJE model is a key ingredient for the numerical fit procedure to determine optimal parameters a and ε for the RJE model with respect to a given raw dataset.

Appendix B.4. Duality Relation for the RJE Model

The above expressions ((A24) and (A25)) provide a hint for a possible duality relation in the RJE model when replacing the auxiliary parameters of (A22) according to $x \to 1/x$ and $y \to -y$. To see this, it is useful to express the Lorenz curve expression ((A14) and (A15)) in terms of the two parameters (x and y), which gives the following nice formula:

$$w_{\mathrm{RJE}}(h) = \frac{W(h,x,y)}{D(a)\varepsilon} \quad \text{with} \quad W(h,x,y) = -\frac{1-x}{y}\ln\left(\frac{1-x\,e^{yh}}{1-x}\right) - xh \tag{A27}$$

where the $W(h,x,y)$ function satisfies the interesting property of $W(h,x,y) = x\,W(h,1/x,-y)$. This means that we have the same Lorenz curves (and te same values of the Gini coefficient) for two different parameter sets ((a,ε) and (a',ε)) if we can find, for a given pair (a,ε), a value of a' (with the same ε value) such that $x(a)/D(a) = 1/D(a')$, $x(a') = 1/x(a)$ and $y(a') = -y(a)$. It is, indeed, possible to satisfy all three relations by choosing $a' = \ln(1 + D(a)/x(a)) = \ln(1 - 1/\mu(a))$. Then, using the implicit Equations (A16) and (A17) (reformulated for the variable of $x = -D\mu$), one can verify that the resulting parameter values for a' , indeed, satisfy $x(a') = 1/x(a)$ and $y'(a) = -y(a)$, showing that the analytical RJE Lorenz curves (A27) (and Gini coefficients as well) between a and a' (both for the same value of ε but with different μ values) are exactly identical.

For example, for the data of the World 2021 Lorenz curve shown in Figure 5, we have the optimal RJE parameters of $a = 4.74$ and $\varepsilon = 0.0113$, corresponding to the blue curve in Figure 5. Using the duality relation, we find that there is a second solution for optimal RJE parameters with $a' = 8.24$ and $\varepsilon' = \varepsilon = 0.0113$, which gives the identical RJE Lorenz curve as for $a = 4.74$. This is also confirmed by the numerical code that determines the optimal a value (by choosing a different start value for the iterative procedure of this code).

Appendix B.5. RJE Energies' Dependence on Cumulated Household

In the RJE model (at finite N), the energies (corresponding to individual wealth), i.e., $w_m = E_m$ as a function of the mode index (m), are simply given by the formula expressed as $E_m = (e^{am/N} - 1)/D(a)$ for $m = 0, 1, \ldots, N-1$. However, a non-trivial but very interesting quantity is the dependence of E_m on the cumulated household ($h(m) = \sum_{k=1}^{m} \rho_k$) associated with the index (m). To obtain this dependence for a finite m and some given value of h, one has to find the specific index (m, as a function of h) such that $h(m) \le h < h(m+1)$ and take $E_{m(h)}$ (or some interpolation value between $E_{m(h)}$ and $E_{m(h)+1}$) for this particular index ($m(h)$). This procedure is for a finite N and is not particularly exact; even for $N = 10{,}000$, we may have a significant condensation effect where the first values of $h(m = 1)$ and $h(m = 2)$ are rather large (not $\sim 1/N$ but closer to ~ 0.1).

In the continuous limit of $N \to \infty$ using the above results, we now have an easy answer for this household dependence of the RJE energy. We simply take the smooth function of $E_s(s) = (e^{as} - 1)/D(a)$, which is the RJE energy as a function of the continuous rescaled index ($s = m/N$) and replace it with $s \to s(h)$ as given above in the analytic expression (A14). This gives the following function:

$$E_h(h) = E_s(s(h)) = \frac{1}{D(a)}\left(\frac{1}{e^{-as(h)}} - 1\right) = \mu\frac{1 - \exp\left(\frac{a(1+\mu D(a))h}{D(a)(\varepsilon-\mu)}\right)}{1 + \mu D(a)\exp\left(\frac{a(1+\mu D(a))h}{D(a)(\varepsilon-\mu)}\right)}, \tag{A28}$$

where we actually use the intermediate expression (A13) to replace $e^{-as(h)}$, which is more convenient.

Note that we can also use the finite N Lorenz-curve construction procedure of Section 2.2 to obtain the following:

$$\frac{w(m+1)-w(m)}{h(m+1)-h(m)} = \frac{\frac{E_m}{E}\rho_m}{\rho_m} = \frac{E_m}{E} \quad \Rightarrow \quad E_h(h) = \varepsilon w'(h) \tag{A29}$$

taking the limit of $N \to \infty$ corresponding to $h(m+1) \to h(m)$ such that we have the $w'(h)$ derivative. This results means that $E_h(h)$ is related to the derivative of the Lorenz curve ($w(h)$, with an additional factor of $E = \varepsilon$). This can also be confirmed by a direct calculation of the derivative ($w'(h)$) from the Lorenz-curve expression (A15) (combined with (A14)), which reproduces exactly $E_h(h)/\varepsilon$ with $E_h(h)$ given by (A28). We mention that we used the result (*A28*) to compute the RJE GDP values used in Figure 13 for each country according to $w_m^{(\mathrm{RJE})} = E_h((m-0.5)/212)$, where $m = 1, 2, \ldots, 212$ is the country index ($m = 212$ for the country with maximal GDP and $m = 1$ for the country with minimal GDP). Here, RJE parameters a and ε are obtained by an optimal curve fit for the Lorenz curve of the original GDP UN data. See also the next appendix section for some details on this point.

Appendix B.6. Cumulative Distribution Function

Finally, we want to compute the cumulative distribution function ($C(w_m)$) which gives the probability/fraction of households with individual wealth larger than w_m. This is just $1 - h(s)$, with $h(s)$ being the cumulated household as a function of the index variable (s) given in (A11), provided s is determined such that the individual wealth/energy ($w_m = E_m$), indeed, corresponds to the index value (s), i.e.,:

$$w_m = E_m = E_s(s) = \frac{e^{as}-1}{D(a)} \quad \Rightarrow \quad e^{as} = 1 + D(a)w_m \quad \Rightarrow \quad e^{-as} = \frac{1}{1+D(a)w_m}\,. \tag{A30}$$

Inserting this expression for e^{-as} in (A11), we get (using $b = 1 + \mu D(a)$)

$$C_{\mathrm{RJE}}(w_m) = 1 - \frac{(\varepsilon-\mu)D(a)}{ab}\ln\left(\frac{1-be^{-as}}{1-b}\right) = 1 - \frac{(\varepsilon-\mu)D(a)}{ab}\ln\left(\frac{1-b\frac{1}{1+D(a)w_m}}{1-b}\right) \tag{A31}$$

$$= 1 - \frac{\varepsilon-\mu}{a(D^{-1}(a)+\mu)}\ln\left(\frac{1-\mu^{-1}w_m}{1+D(a)w_m}\right). \tag{A32}$$

From this analytical result, we can deduceseveral limiting cases. First, for the RJS case of $a \to 0$ (where $C(w_m)$ was not discussed in the first appendix section), we get

$$C_{\mathrm{RJS}}(w_m) = 1 - (\varepsilon-\mu)\ln\left(1-\mu^{-1}w_m\right). \tag{A33}$$

Furthermore, from (A32) (and similarly for (A33)), we obtain the linear expansion for (very) small w_m values, i.e.,

$$C_{\mathrm{RJE}}(w_m) \approx 1 - \frac{(\varepsilon-\mu)(-\mu^{-1}-D(a))}{a(D^{-1}(a)+\mu)}w_m = 1 - \frac{(\varepsilon-\mu)}{a}(-\mu^{-1}D(a))\,w_m \tag{A34}$$

which is only valid for $w_m \ll \min(-\mu, D^{-1}(a))$, which is typically a very small range, especially for small ε values with even smaller values of $-\mu$. Therefore, this linear regime has only a very limited importance.

It is more interesting to consider the case of a relatively large value of a (e.g., $a \sim 7$ or similar) such that $e^a \approx D(a) \gg 1$, where the limit is $w_m \gg \max(-\mu, D^{-1}(a))$, where typically, $\max(-\mu, D^{-1}(a)) \ll 1$. Then, in (A32), we can apply a different expansion in $1/w_m$:

$$C_{\mathrm{RJE}}(w_m) = 1 - \frac{\varepsilon-\mu}{a(D^{-1}(a)+\mu)} \ln\left(\frac{1-\mu^{-1}w_m}{1+D(a)w_m}\right) \tag{A35}$$

$$= 1 - \frac{\varepsilon-\mu}{a(D^{-1}(a)+\mu)} \left[-\ln(-\mu D(a)) + \ln\left(\frac{1-\mu w_m^{-1}}{1+D^{-1}(a)w_m^{-1}}\right)\right] \tag{A36}$$

$$\approx C_1 + \frac{C_2}{w_m} \quad \text{with} \quad C_2 = \frac{\varepsilon-\mu}{a} \tag{A37}$$

and

$$C_1 = 1 + \frac{\varepsilon-\mu}{a(D^{-1}(a)+\mu)} \ln(-\mu D(a)) \approx \ldots \approx -\frac{\varepsilon-\mu}{a} = -C_2 \tag{A38}$$

where "…" represent some simplification steps using twice the implicit μ Equation (A16) (in both ways) and the replacement is $D^{-1}(a) \approx e^{-a}$.

In summary, we find the following quite simple expression:

$$C_{\mathrm{RJE}}(w_m) \approx \frac{\varepsilon-\mu}{a}\left(\frac{1}{w_m} - 1\right) \tag{A39}$$

which is valid in the full interval of $w_m \in [w_{\min}, 1]$, where $w_{\min}$ is some value with $w_{\min} \gg \max(-\mu, D^{-1}(a))$.

For example, in the left panel of Figure 20, the RJE fit for the Bitcoin data of 2013.Q1 (dashed blue line) is very close to (A39) for $w_m > 3 \times 10^{-5}$, and the constant term in (A39) assures the correct behavior up to $w_m \to 1$, where $C_{\mathrm{RJE}}(w_m) \to 0$. If we consider the smaller interval of $w_m \in [3 \times 10^{-5}, 10^{-1}]$, then we can also neglect the constant term in (A39) such that we have a pure power law of $C_{\mathrm{RJE}}(w_m) \approx C_2 w_m^{-1}$ corresponding to the straight blue dashed line in the left panel of Figure 20 (for this specific interval). In general, this pure power-law regime with an exponent of -1 is only visible for large values of a, the appropriate interval for w_m and small values of ε (i.e values of $G \sim 0.9$–0.95). For more modest values of a or slightly larger values of ε, we also hae an intermediate regime with a decay of $\sim \ln(1/w_m)$ (especially for the pure RJS case with $a = 0$). The more refined approximation (A39) with the constant term (which gives curved behavior in a double-logarithmic representation) is, in general, quite accurate for a suitable interval of $[w_{\min}, 1]$, even with more modest values of a.

We mention that the $C(w_m)$ curves for the RJE model (in the continuous limit) presented in several figures of this work are based on the exact expression (A32) or an equivalent reformulation (e.g., using (A16)). The $C(w_m)$ curves for the finite-N RJE model (or some real data) are typically obtained by plotting the (rescaled) energy/individual wealth ($E_m \sim w_m$) versus $1 - h(m)$. It is also possible to reconstruct a $C(w_m)$ curve from a Lorenz curve, but this requires good-quality data and the (discrete) derivative of $w(h)$ to obtain $w_m \sim E_m \sim w'(h)$.

Appendix C. Additional Data for GDP of Countries

Here, we show additional figures for the GDP of countries and some additional explanations about the data shown in Figure 13. In Figure 9, we compare the Lorenz curves of UN GDP data of 1973 and 2023 with theoretical Lorenz curves for the RJS and RJE models (with optimal values of a for the RJE case). In this context, we attribute to each of the 212 countries (for the 2023 data) an identical household fraction of $\Delta h = 1/212$, which can be seen by the equidistant red data points (with respect to the x-axis). However, the data points for the RJS/RJE models correspond to energy modes E_k, $k = 0, 1, \ldots, N-1$, where, e.g., $N = 10{,}000$ (for the case of Figure 9) with non-uniform ρ_k values for the household fraction for a given mode (k) (also called "agent" with index k) given by the following RJ

formula: $\rho_k = T/(E_k - \mu)$. In particular, for larger values of k, the value of ρ_k decays, and the density of RJE data points on the x-axis increases.

In this context, one can ask the question of how many agents (k-modes) of the RJE model correspond to a particular country (m; $m = 1, \ldots, 212$). Let $h^{(\mathrm{GDP})}(m) = m/212$ be the cumulated household variable of the raw GDP data and $h^{(\mathrm{RJE})}(k) = \sum_{l=0}^{k-1} \rho_l$ (such that $h^{(\mathrm{RJE})}(k = N) = 1$) be the cumulated household variable for the RJE model (e.g., for the case with optimal fit values for a and ε with respect to the GDP data).

Then, the number of agents (N_m) associated with country m is the number of $h^{(\mathrm{RJE})}(k)$ values that satisfy the following inequality: $h^{(\mathrm{GDP})}(m-1) \leq h^{(\mathrm{RJE})}(k) < h^{(\mathrm{GDP})}(m)$. This number ($N_m$) typically increases with m and k, since ρ_k (the difference between two $h^{(\mathrm{RJE})}(k)$ values) decreases. Actually, at $N = 10{,}000$, the first values of $h^{(\mathrm{RJE})}(k)$ ($k = 1, 2, \ldots$) cover several (∼4–5) countries (due to the effect of RJ condensation), and much larger values of N are required to reach the continuous limit. Using the analytical expression (A14) for the index variable ($s(h)$, dependent on the cumulated household (h)), we can compute the number (N_m) or, more precisely, the fraction of $f_m = N_m/N$ according to $f_m = s((m+1)/212) - s(m/212)$.

At the same time, for a given country (m), we can also search the RJE energy mode such that $h^{(\mathrm{RJE})}(k_m)$ is in the middle of the interval $[h^{(\mathrm{GDP})}(m-1), h^{(\mathrm{GDP})}(m)[$ (with best possible precision). This gives a virtual RJE GDP value of $w_m = CE_{k_m}$ for country m , where the constant (C) is determined such that $\sum_m w_m = 1$ (sum-normalized RJE GDP values). Using another analytic result (A28) of Appendix B for the RJE energy dependence ($E_h(h)$) on the cumulated household (h), we directly obtain $w_m = CE_h((m-0.5)/212)$ (for $m = 1, \ldots, 212$ and sum normalization to fix C). These particular effective RJE GDP (sum normalized) wealth values were used for the world map-type figure (Figure 13).

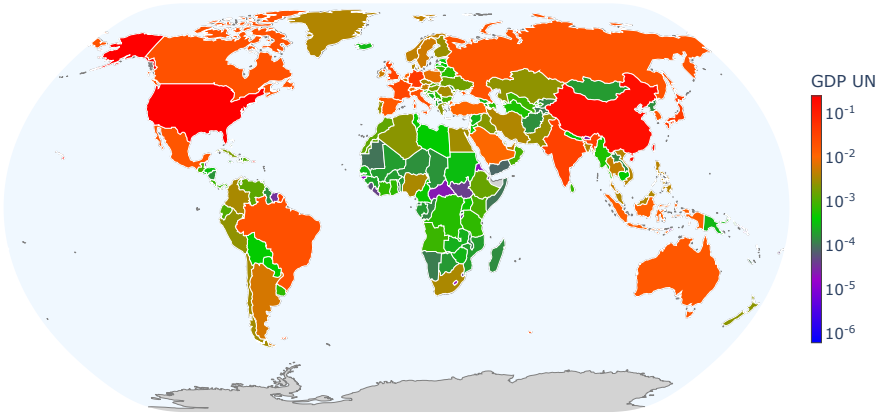


Figure A3. Same as Figure 13, with real GDP data from UN 2023; color normalization is the same as in Figure 13.

Figure A3 is of the same style as Figure 13, but it shows, for comparison, the (sum-normalized) real GDP UN data for 2023 (instead of the RJE GDP values).

Furthermore, Figure A4 shows the relative difference between the two GDP quantities (difference on a logarithmic scale). Examples of countries with large differences are Germany, Japan and India, with larger RJE GDP values (by 58%, 35% and 28% respectively) and China and Australia, with smaller RJE GPD values (by 37% and 18% respectively, both in comparison with the real UN data).

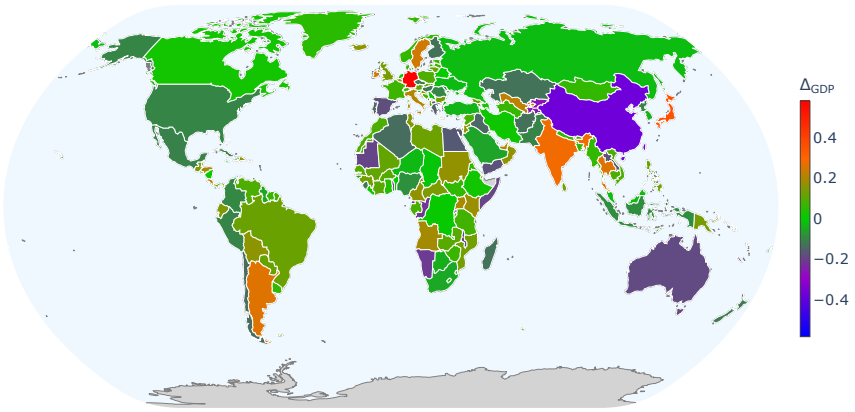


Figure A4. Color shows the relative difference (Δ_{GDP}) in GDP values between real data (shown in Figure A3) and the RJE GDP values (shown in Figure 13); here, $\Delta_{GDP} = \ln(w_m^{(\mathrm{RJE})}) - \ln(w_m^{(\mathrm{UN})}) \approx \Delta w_m / \bar{w}_m$ with $\Delta w_m = w_m^{(\mathrm{RJE})} - w_m^{(\mathrm{UN})}$ and $\bar{w}_m = (w_m^{(\mathrm{RJE})} + w_m^{(\mathrm{UN})})/2$.

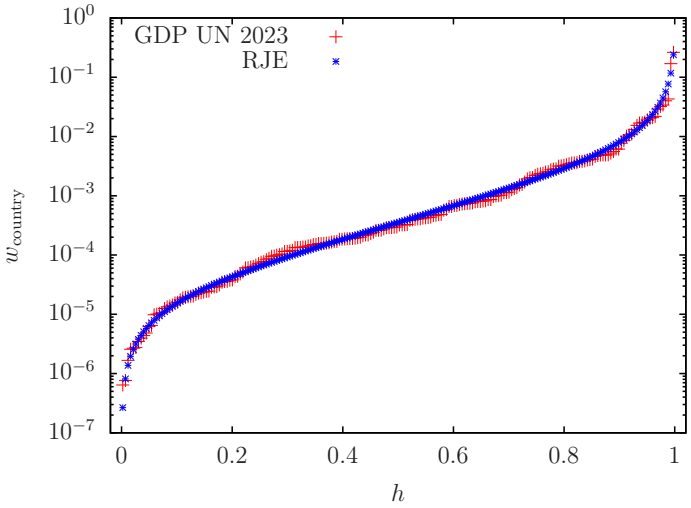


Figure A5. Sum-normalized country GPD wealth on a logarithmic scale versus the rescaled country index ($h = (m - 0.5)/212$) for $m = 1, \ldots, 212$ obtained by ordering the world countries by increasing GDP. The red data points (+ symbols) correspond to the real UN 2023 GDP data, and the blue data points ($*$ symbols) correspond to the RJE GDP values for the optimal GDP RJE fit used in Figure 13 (see text for details). (Data from [53])

Figure A5 shows a direct comparison of the (sum-normalized) wealth values (w_m) between the RJE GDP values and the UN data as a function of the (rescaled) country index and with a logarithmic scale for w_m. The two curves are close, as expected, but for some countries/data points, there are significant deviations. Essentially, the RJE GDP curve in Figure A5 corresponds to a smoothed UN data curve. Note that the differences of $\ln(w_m)$ between the two cases correspond to the values used in Figure A4.

References

1. Landau, L.D.; Lifshitz, E.M. *Statistical Mechanics*; Wiley: New York, NY, USA, 1976.
2. Fixsen, D.J. The temperature of the cosmic microwave background. *Astrophys. J.* **2009**, *707*, 916. [CrossRef]
3. Wikipedia Contributors, Cosmic Microwave Background. 2026. Available online: https://en.wikipedia.org/wiki/Cosmic_microwave_background (accessed on 9 February 2026).
4. Mantegna, R.N.; Stanley, H.E. *An Introduction to Econophysics: Correlations and Complexity in Finance*; Cambridge University Press: Cambridge, UK, 1999.
5. Dragulescu, A.; Yakovenko, V. Statistical mechanics of money. *Eur. Phys. J. B* **2000**, *17*, 723. [CrossRef]

6. Yakovenko, V.M.; Rosser, J.B. Colloquium: Statistical mechanics of money, wealth, and income. *Rev. Mod. Phys.* **2009**, *81*, 1703. [CrossRef]
7. Piketty, T. *Capital in the Twenty-First Century*; Belknap Press of Harvard University Press: Cambridge, MA, USA, 2014.
8. Chancel, L.; Piketty, T.; Saez, E.; Zucman, G. *World Inequality Report 2022*; World Inequality Lab: Paris, France. Available online: https://wir2022.wid.world (accessed on 12 April 2026).
9. Roach, B.; Rajkanikar, P.J.; Goodwin, N.; Harris, J. Social and Economic Inequality. An ECI Teaching Module on Social and Environmental Issues, Economics in Context Initiative, Global Development Policy Center, Boston University. 2003. Available online: https://www.bu.edu/eci/files/2023/05/Inequality-Module-2023.pdf (accessed on 9 February 2025).
10. Lifshitz, E.M.; Pitaevskii, L.P. *Physical Kinetics*; Pergamon Press: New York, NY, USA, 1995.
11. Angle, J. The surplus theory of social stratification and the size distribution of personal Wealth. *Soc. Forces* **1986**, *65*, 293. [CrossRef]
12. Ispolatov, S.; Krapivsky, P.L.; Redner, S. Wealth distributions in asset exchange models. *Eur. Phys. J. B* **1998**, *2*, 267. [CrossRef]
13. Bouchaud, J.-P.; Mezard, M. Wealth condensation in a simple model of economy. *Physica A* **2000**, *282*, 536. [CrossRef]
14. Chakrabarti, B.K.; Chakraborti, A.; Chakravarty, S.R.; Chatterjee, A. *Econophysics of Income and Wealth Distributions*; Cambridge University Press: New York, NY, USA, 2013.
15. Boghosian, B.M.; Devitt-Lee, A.; Johnson, M.; Li, J.; Marcq, J.A.; Wang, H. Oligarchy as a phase transition: The effect of wealth-attained advantage in a Fokker–Planck description of asset exchange. *Phys. A* **2017**, *476*, 15. [CrossRef]
16. Boghosian, B.M. The inescapable casino. *Sci. Am.* **2019**, *321*, 70. [CrossRef] [PubMed]
17. Lorenz, M.O. Methods of measuring the concentration of wealth. *Q. Publ. Am. Stat. Assoc.* **2009**, *9*, 209–219. [CrossRef]
18. Gini, C. *Sulla Misura Della Concentrazione e Della Variabilit'a Dei Caratteri*; C. Ferrari: Clusone, Italy, 1914; Volume 73, pp. 1203–1248. Available online: https://www.dss.uniroma1.it/RePec/mtn/articoli/2005-1-1.pdf (accessed on 12 April 2026).
19. Wikipedia. List of Sovereign States by Wealth Inequality. Available online: https://en.wikipedia.org/wiki/List_of_sovereign_states_by_wealth_inequality (accessed on 12 April 2026).
20. Frahm, K.M.; Shepelyansky, D.L. Wealth Thermalization Hypothesis and Social Networks. *arXiv* **2025**, arXiv:2506.17720.
21. Marx, K. *Das Kapital: Kritik der politischen Oekonomie. Vol. 1: Der Produktionsprozess des Kapitals*, 1st ed.; Verlag von Otto Meissner: Hamburg, Germany, 1867; Volume 1. [CrossRef]
22. Lenski, G.E. *Power and Privilege: A Theory of Social Stratification*; Univ. North Carolina Press: Chapel Hill, NC, USA, 1984.
23. Sanders, P. *Social Class and Stratification*; Routelege: London, UK, 1990.
24. Kerbo, H.R. *Social Stratification and Inequality: Class Conflict in Historical, Comparative, and Global Perspective*, 9th ed.; Routledge: New York, NY, USA, 2017.
25. Wikipedia. Social Stratification. Available online: https://en.wikipedia.org/wiki/Social_stratification (accessed on 12 April 2026).
26. Frahm, K.M.; Shepelyansky, D.L. Dynamical thermalization and turbulence in social stratification models. *CHAOS* **2026**, *35*, 073117.
27. Zakharov, V.E.; L'vov, V.S.; Falkovich, G. *Kolmogorov Spectra of Turbulence*; Springer: Berlin/Heidelberg, Germany, 1992.
28. Frahm, K.M.; Shepelyansky, D.L. Nonlinear perturbation of Random Matrix Theory. *Phys. Rev. Lett.* **2023**, *131*, 077201. [CrossRef] [PubMed]
29. Ermann, L.; Chepelianskii, A.D.; Shepelyansky, D.L. Dynamical thermalization, Rayleigh-Jeans condensate, vortexes and wave collapse in quantum chaos fibers and fluid of light. *J. Phys. A Math. Theor.* **2026**, *59*, 055702. [CrossRef]
30. Chirikov, B.V. A universal instability of many-dimensional oscillator systems. *Phys. Rep.* **1979**, *52*, 263–379. [CrossRef]
31. Lichtenberg, A.; Lieberman, M. *Regular and Chaotic Dynamics*; Springer: NewYork, NY, USA, 1992.
32. Arnold, V.; Avez, A. *Ergodic Problems of Classical Mechanics*; Benjamin: NewYork, NY, USA, 1968.
33. Cornfeld, I.P.; Fomin, S.V.; Sinai, Y.G. *Ergodic Theory*; Springer: NewYork, NY, USA, 1982.
34. Krupa, K.; Tonello, A.; Barthelemy, A.; Shalaby, B.M.; Bendahmane, A.; Millot, G.; Wabnitz, S. Observation of geometric parametric instability induced by the periodic spatial self-imaging of multimode waves. *Phys. Rev. Lett.* **2016**, *116*, 183901. [CrossRef] [PubMed]
35. Connaughton, C.; Josserand, C.; Picozzi, A.; Pomeau, Y.; Rica, S. Condensation of classical nonlinear waves. *Phys. Rev. Lett.* **2005**, *95*, 263901. [CrossRef] [PubMed]
36. Picozzi, A.; Garnier, A.; Hansson, J.; Suret, T.; Randoux, P.; Millot, S.; Christodoulides, G. Optical wave turbulence: Towards a unified nonequilibrium thermodynamic formulation of statistical nonlinear optics. *Phys. Rep.* **2014**, *542*, 1. [CrossRef]
37. Baudin, K.; Fusaro, A.; Krupa, K.; Garnier, J.; Rica, S.; Millot, G.; Picozzi, A. Classical Rayleigh-Jeans condensation of light waves: Observation and thermodynamic characterization. *Phys. Rev. Lett.* **2020**, *125*, 244101. [CrossRef] [PubMed]
38. Podivilov, E.V.; Mangini, F.; Sidelnikov, O.S.; Ferraro, M.; Gervaziev, H.; Kharenko, D.S.; Zitelli, M.; Fedoruk, M.P.; Babin, S.A.; Wabnitz, S. Thermalization of orbital angular momentum beams in multimode optical fibers. *Phys. Rev. Lett.* **2022**, *128*, 243901. [CrossRef] [PubMed]
39. Pourbeyram, H.; Sidorenko, P.; Wu, F.O.; Bender, N.; Wright, L.; Christodoulides, D.N.; Wise, F. Direct observations of thermalization to a Rayleigh–Jeans distribution in multimode optical fibres. *Nat. Phys.* **2022**, *18*, 685. [CrossRef]

40. Baudi, K.; Garnier, J.; Fusaro, A.; Berti, N.; Michel, C.; Krupa, K.; Millot, G.; Picozzi, A. Observation of light thermalization to negative-temperature Rayleigh-Jeans equilibrium states in multimode optical fibers. *Phys. Rev. Lett.* **2023**, *130*, 063801. [CrossRef] [PubMed]
41. Fröhlich, H. Bose condensation of strongly excited longitudinal electric modes. *Phys. Lett. A* **1968**, *26A*, 402. [CrossRef]
42. Fröhlich, H. Long-range coherence and energy storage in biological systems. *Int. J. Quantum Chem.* **1968**, *II*, 641. [CrossRef]
43. Nazarenko, S. *Wave Turbulence*; Springer: Berlin/Heidelberg, Germany, 2011.
44. Evans, M.R.; Majumdar, S.N.; Pagonabarraga, I.; Trizac, E. Condensation transition in polydisperse hard rods. *J. Chem. Phys.* **2010**, *132*, 014102. [CrossRef] [PubMed]
45. Szavits-Nossan, J.; Evans, M.R.; Majumdar, S.N. Constraint driven condensation in large fluctuations of linear statistics. *Phys. Rev. Lett.* **2014**, *112*, 020602. [CrossRef] [PubMed]
46. Filiasi, M.; Livan, G.; Marsili, M.; Peressi, M.; Vesselli, E.; Zarinelli, E. On the concentration of large deviations for fat tailed distributions, with application to financial data. *J. Stat. Mech.* **2014**, *2014*, P09030. [CrossRef]
47. Zucman, G. *Hidden Wealth of Nations*; University of Chicago Press: Chicago, IL, USA, 2015.
48. Pareto, V. *Cours D'Économie Politique Professé a L'Université de Lausanne*; Lausanne University: Lausanne, Switzerland, 1897; pp. 1896–1897.
49. Aladangady, A.; Forde, A. Wealth Inequality and the Racial Wealth Gap, FEDS Notes Oct 22. 2021. Available online: https://www.federalreserve.gov/econres/notes/feds-notes/2021-index.htm (accessed on 8 June 2025).
50. Cowell, F.; Nolan, B.; Olivera, J.; Van Kerm, P. Wealth, Top Incomes and Inequality. In *National Wealth*; Hamilton, K., Herburn, C., Eds.; Oxford Univ. Press: Oxford, UK, 2017; p. 175.
51. Wikipedia. Gross Domestic Product. Available online: https://en.wikipedia.org/wiki/Gross_domestic_product (accessed on 12 April 2026).
52. Wikipedia. List of Countries by GDP (Nominal). Available online: https://en.wikipedia.org/wiki/List_of_countries_by_GDP_(nominal) (accessed on 12 April 2026).
53. United Nations Statistical Division. National Accounts. Available online: https://unstats.un.org/unsd/snaama/Downloads (accessed on 12 April 2026).
54. Wikipedia. List of Countries by Stock Market Capitalization. Available online: https://en.wikipedia.org/wiki/List_of_countries_by_stock_market_capitalization (accessed on 12 April 2026).
55. Wikipedia. List of Countries by GDP (Nominal) Per Capita. Available online: https://en.wikipedia.org/wiki/List_of_countries_by_GDP_(nominal)_per_capita (accessed on 12 April 2026).
56. Hong Kong Stock Exchange Data of Capitalization of Companies. Available online: https://www.hkex.com.hk/Market-Data/Securities-Prices/Equities?sc_lang=en (accessed on 19 June 2025).
57. Shanghai Stock Exchange Data of Capitalization of Companies. Available online: https://english.sse.com.cn/markets/equities/data/ (accessed on 18 November 2025).
58. London Stock Exchange Data of Capitalization of Companies. Available online: https://www.londonstockexchange.com/reports?trkcode=lsehomstatstab=issuers (accessed on 15 May 2026).
59. Ermann, L.; Frahm, K.M.; Shepelyansky, D.L. Google matrix of Bitcoin network. *Eur. Phys. J. B* **2018**, *91*, 127. [CrossRef]
60. Brugere I. Available online: https://github.com/ivanbrugere (accessed on 5 June 2026).
61. Available online: https://blockchain.info/ (accessed on 5 June 2026).
62. Ron, D.; Shamir, A. Quantitative analysis of the full bitcoin transaction graph. In *Financial Cryptography and Data Security*; Sadeghi, A.R., Ed.; FC 2013; Springer: Berlin/Heidelberg, Germany, 2013; Volume 7859, p. 6.
63. Biryukov, A.; Khovratovich, D.; Pustogarov, I. Deanonymisation of clients in Bitcoin P2P network. In Proceedings of the 21st ACM Conference on Computer and Communications Security (CCS '14), Scottsdale, AZ, USA, 3–7 November 2014; p. 15.
64. Bohannon, J. The Bitcoin busts. *Science* **2016**, *351*, 1144.
65. Kim, Z.Y.; Park, J.-H. Distinguishable cash, bosonic bitcoin, and fermionic non-fungible token. *Front. Phys.* **2023**, *11*, 1113714. [CrossRef]
66. Park, C.; Tessone, C.J.; Zhang, Y.; Park, J.-H. Empirical confirmation of bosonic wealth statistics in Bitcoin UTXOs. *arXiv* **2026**, arXiv:2605.12853.
67. Ermann, L.; Shepelyansky, D.L. Google matrix of the world trade network. *Acta Phys. Pol. A* **2011**, *120*, A158. [CrossRef]
68. Ermann, L.; Shepelyansky, D.L. Google matrix analysis of the multiproduct world trade network. *Eur. Phys. J. B* **2015**, *88*, 84. [CrossRef]
69. Zucman, G. Globalisation, taxation and inequality. *Fisc. Stud.* **2023**, *44*, 229–235. [CrossRef]

Disclaimer/Publisher's Note: The statements, opinions and data contained in all publications are solely those of the individual author(s) and contributor(s) and not of MDPI and/or the editor(s). MDPI and/or the editor(s) disclaim responsibility for any injury to people or property resulting from any ideas, methods, instructions or products referred to in the content.